Biochimica et Biophysica Acta 1843 (2014) 1309–1324

Contents lists available at ScienceDirect

Biochimica et Biophysica Acta

journal homepage: www.elsevier.com/locate/bbamcr

CDK5-mediated phosphorylation of p19INK4d avoids DNA damage-induced neurodegeneration in mouse hippocampus and prevents loss of cognitive functions

María Florencia Ogara [a], Laura M. Belluscio [a], Verónica de la Fuente [b], Bruno G. Berardino [a], Silvina V. Sonzogni [a], Laura Byk [a], Mariela Marazita [a], Eduardo T. Cánepa [a,*]

[a] Laboratorio de Biología Molecular, Departamento de Química Biológica, Ciudad Universitaria, Pabellón II piso 4, 1428 Ciudad de Buenos Aires, Argentina
[b] Laboratorio de Neurobiología de la Memoria, Departamento de Fisiología, Biología Molecular y Celular, Facultad de Ciencias Exactas y Naturales, Universidad de Buenos Aires, Ciudad Universitaria, Pabellón II piso 4, 1428 Ciudad de Buenos Aires, Argentina

ARTICLE INFO

Article history:
Received 12 October 2013
Received in revised form 26 March 2014
Accepted 27 March 2014
Available online 3 April 2014

Keywords:
DNA damage
Neurodegeneration
Learning and memory
Neocarzinostatin
Beta amyloid peptide
Apoptosis

ABSTRACT

DNA damage, which perturbs genomic stability, has been linked to cognitive decline in the aging human brain, and mutations in DNA repair genes have neurological implications. Several studies have suggested that DNA damage is also increased in brain disorders such as Alzheimer's disease, Parkinson's disease and amyotrophic lateral sclerosis. However, the precise mechanisms connecting DNA damage with neurodegeneration remain poorly understood. CDK5, a critical enzyme in the development of the central nervous system, phosphorylates a number of synaptic proteins and regulates dendritic spine morphogenesis, synaptic plasticity and learning. In addition to these physiological roles, CDK5 has been involved in the neuronal death initiated by DNA damage. We hypothesized that p19INK4d, a member of the cell cycle inhibitor family INK4, is involved in a neuroprotective mechanism activated in response to DNA damage. We found that in response to genotoxic injury or increased levels of intracellular calcium, p19INK4d is transcriptionally induced and phosphorylated by CDK5 which provides it with greater stability in postmitotic neurons. p19INK4d expression improves DNA repair, decreases apoptosis and increases neuronal survival under conditions of genotoxic stress. Our in vivo experiments showed that decreased levels of p19INK4d rendered hippocampal neurons more sensitive to genotoxic insult resulting in the loss of cognitive abilities that rely on the integrity of this brain structure. We propose a feedback mechanism by which the neurotoxic effects of CDK5-p25 activated by genotoxic stress or abnormal intracellular calcium levels are counteracted by the induction and stabilization of p19INK4d protein reducing the adverse consequences on brain functions.

1. Introduction

Neuronal apoptosis is an essential process in the development of the nervous system especially during synaptogenesis. Through development, the nervous system is generated with an excess number of neurons. This production in excess is followed by apoptosis during a restricted developmental period, leading to the elimination of as much as half of the originally produced cells [1–3]. This massive apoptosis is crucial to shaping the complex architecture of the brain and establish the neuronal circuits needed for the execution of motor function, learning and memory among other tasks. It is supposed that only those neurons that receive the proper trophic input from their targets will survive [4–6].

In addition to the extensive naturally occurring cell death in the developing nervous system, neuronal apoptosis is a prominent feature in a number of acute and chronic neurological diseases including stroke, Alzheimer's disease, and amyotrophic lateral sclerosis [7,8]. In general, neuronal apoptosis in these disorders seems not to be the result of trophic factor withdrawal, but of toxic insults such as abnormal protein aggregates and free-radical generation.

DNA damage may also be engaged in numerous conditions involving neuronal death. The nervous system is very sensitive to DNA damage, particularly in comparison with other tissues that contain non-replicating cell types. There are some unique properties of the nervous system that may account for this relative sensitivity. The brain metabolizes ~20% of the oxygen consumed but has lower ability than other body parts to neutralize reactive oxygen species (ROS) and neurons are particularly susceptible to oxidative stress. This high oxidative load

Abbreviations: ATRA, all-*trans*-retinoic acid; CDK, cyclin-dependent kinase; ODN, oligodeoxynucleotide; NCS, neocarzinostatin; ROS, reactive oxygen species; UDS, unscheduled DNA synthesis

* Corresponding author at: Departamento de Química Biológica, Facultad de Ciencias Exactas y Naturales, Ciudad Universitaria Pabellón II piso 4, 1428 Ciudad de Buenos Aires, Argentina. Tel./fax: +54 11 45763342.
E-mail address: ecanepa@qb.fcen.uba.ar (E.T. Cánepa).

http://dx.doi.org/10.1016/j.bbamcr.2014.03.026
0167-4889/

presumably generates free radicals, which increases DNA damage [9,10].

Evidence suggests that DNA damage may be a central event in neurodegeneration [11]. For instance, DNA strand breaks occur as an early event after reperfusion of the ischemic brain, and DNA lesions have been reported in Parkinson's and Alzheimer's diseases [12,13]. Furthermore, congenital syndromes with DNA repair gene mutations, such as ataxia telangiectasia and Werner's syndrome, display a progressive neurodegeneration phenotype [11]. In addition, DNA damage is involved in the aging of the human brain, which suggests that DNA damage may play a role in age-dependent neurodegenerative diseases as well [14,15]. These observations demonstrate the importance of maintaining DNA integrity in the mature brain.

Cyclin-dependent kinase 5 (CDK5) is a member of the cyclin-dependent kinase family of serine/threonine kinases that is critical for the development of the central nervous system. CDK5 is expressed ubiquitously in many tissues; however, its activity is restricted primarily to the nervous system due to neuron-specific expression of its activator molecules p35 and p39 [16,17]. CDK5 phosphorylates a number of synaptic proteins and regulates dendritic spine morphogenesis, synaptic plasticity and learning [18]. Nevertheless, in addition to these physiological roles, CDK5 also has a dark side [19]. Evidence suggests that CDK5 becomes an inducer of death when its activator p35 is cleaved into a smaller p25 form by calpains and may play a role in the pathogenesis of neurodegenerative disorders, such as Alzheimer's disease and amyotrophic lateral sclerosis [20]. Accumulation of p25 and involvement of CDK5 have been observed in neurons treated with excitotoxins, β-amyloid, and oxidative stress, as well as in animal models of stroke and Parkinson's disease [21]. In these conditions, calpain-directed proteolysis of p35 deprives the membrane-associated p35 of an N-terminal myristoylated membrane tether, releasing p25 into the cytoplasm. More recently, CDK5 has been involved in neuronal death initiated by DNA damage [22].

Recent works have reported that p16INK4a and p19INK4d (hereafter referred to as p19), two proteins from the INK4 family, could be involved in the cellular response to genotoxic agents [23–25]. In particular, there are strong evidences that p19 plays a crucial role in regulating genomic stability and cell viability. Notably, improvement of DNA repair in cells that overexpress p19 inversely correlates with the apoptosis triggered by DNA damage [26]. These results suggest that, in addition to its role in improving DNA repair, p19 negatively modulates DNA damage-induced apoptosis in mammalian cells. On this matter, recent studies performed in p19 null mice have demonstrated that the absence of p19 renders cells sensitive to apoptotic and autophagic cell death [27].

INK4 family members are differentially expressed during development [28]. p19 is expressed at high levels within the central nervous system from embryonic day 11.5 onward. During the development of the neocortex asymmetric division gives rise to differentiated neurons that express p19, expression that continues in postmitotic neurons and the adult brain, including the hippocampus, cortex, cerebellum and brainstem [29,30]. The described ability of p19 to maintain genomic integrity and its sustained expression in neurons allow us to hypothesize that this protein is involved in a neuroprotective mechanism activated in response to genotoxic damage.

In the present study we demonstrated that, in response to genotoxic damage or increased levels of intracellular calcium, p19 is induced and phosphorylated in differentiated human neuroblastoma SH-SY5Y cells and in the primary cultures of neurons from rat hippocampus. Genotoxic stress increases CDK5 activity, which, in turn, phosphorylates p19 protein providing it with greater stability. We demonstrated that p19 improves DNA repair, decreases apoptosis and increases neuronal survival under conditions of genotoxic stress. Our in vivo experiments showed that decreased levels of p19 rendered hippocampal neurons that are more sensitive to genotoxic insult resulting in the loss of the cognitive abilities rely on the integrity of this neural structure. The results presented herein describe a mechanism by which p19 protein participates in the maintenance of genomic integrity in neuronal cells.

2. Materials and methods

2.1. Cell cultures and experimental treatments

The human neuroblastoma cell line SH-SY5Y (ATCC, CRL-2266) was grown in Dulbecco's modified Eagle medium (45%) and HAM F-12 (45%) (DMEM/F12; Invitrogen) supplemented with 10% fetal bovine serum (FBS), 1% penicillin/streptomycin, 2 mM glutamine and 1 mM sodium pyruvate (Invitrogen) at 37 °C in a humidified 5% CO_2 atmosphere. The mouse neuroblastoma Neuro-2a (ATCC, CCL-131) and the human embryonic kidney HEK293 (ATCC, CRL-1537) cell lines were maintained in Dulbecco's modified Eagle medium and similarly supplemented. SH-SY5Y cells were differentiated to a neuronal phenotype by growth in DMEM/F12 with 0.2% FBS plus 1 μM ATRA for 7 days.

Primary hippocampal cell cultures were established from E18–E19 embryos aseptically removed from pregnant Wistar rats. Dissociated cultures of hippocampal pyramidal cells from embryonic rat brain tissue were then prepared as described previously [31]. Briefly, hippocampi were treated with trypsin (0.25% for 15 min at 37 °C), washed with a Ca- and Mg-free Hank's balanced solution, and dissociated by repeated passages through a constricted Pasteur pipette. The nerve cell suspensions were then plated on culture dishes coated with poly-D-lysine (1 μg/ml; Sigma-Aldrich). After plating, the cells were incubated for 2–3 h in DMEM containing 10% FBS to enable the neurons to attach to the substrate. The medium was replaced with Neurobasal™ medium (GIBCO) containing 1% N2 and 2% B27 serum-free supplements (GIBCO), and the cultures were maintained in a humidified 37 °C incubator with 5% CO_2.

β-Amyloid peptide (amyloid β-protein fragment 25–35, Sigma) was added in a final concentration of 10 μM for the indicated period of time. NCS (Sigma-Aldrich) was added in a final concentration of 100 ng/ml (unless otherwise indicated) for the indicated period of time. Camptothecin was used in a final concentration of 1 μM for the indicated period of time. UVC light was used in some cases to induce DNA damage. Cells were irradiated in open-dishes with the corresponding 40 J/m^2 UVC dose, 254 nm (range 240–280 nm) at room temperature. Following UV-irradiation, the medium was replaced and cells were incubated for the indicated time at 37 °C in a 5% CO_2 humidified incubator along the times indicated in each case.

Antisense oligodeoxynucleotides at a final concentration of 1 μM were used to selectively knock down the expression of different mRNA genes as indicated. All the sequences are described in the Supporting information.

2.2. Cell transfection

Transient transfections were performed with Lipofectamine™ 2000 reagent (Invitrogen) following the manufacturer's protocol. Before transfection 1×10^6 cells were seeded in 60-mm dishes. Six μg of total DNA and/or pBabePuro (0.5 μg) and Lipofectamine™ 2000 (4 μl) were used per dish. Twenty-four hours after transfection, selection was carried on with 1 μg/ml puromycin for 48 h. All the plasmids used are described in the Supporting information.

For the establishment of stable clones, the pMTCB6 vector, containing a NotI–BamHI fragment encoding the human p19 cDNA downstream the metallothionein promoter carrying a selectable neomycin-resistance gene (pMTp19S), was used. The pMTp19AS was constructed cloning the p19 cDNA in the reverse orientation. Transfections were performed using Lipofectamine™ 2000 Reagent (Invitrogen). Twenty-four hours after the transfection cells were replated at low density to isolate single colonies. The clonal cell lines SH-SY5Y empty, SH-SY5Yp19S, SH-SY5Yp19AS, from now on, derived from the transfectants were maintained in selective medium containing 4 mg/ml geneticin disulfate

(G418, Calbiochem-Novabiochem). For metallothionein promoter induction stable transformants were treated with 100 μM $ZnSO_4$ for at least 16 h.

Hippocampal neurons were transfected with the antisense oligodeoxynucleotide to p19 (p19AS) at a final concentration of 400 nM using FuGENE® HD Transfection Reagent (Roche) according to the manufacturer's protocol.

2.3. RNA extraction and Northern blot analysis

RNA extraction and Northern blot analysis were previously described [32]. Briefly, 10–20 μg of total RNA was denatured, electrophoresed in 1% glyoxal–agarose gels, and transferred to nylon membranes (Hybond N, Amersham). Membranes were sequentially hybridized with the indicated [^{32}P]-labeled probes and radioactivity was detected using a PhosphorImager (FujiFilm BAS-1800II).

2.4. Western blot

Total cell lysates and Western blot analysis were carried out as previously described [33]. The following antibodies were used: mouse anti-p19INK4d (P0999-55A, US Biological), mouse anti-p19INK4d (ZP002, Invitrogen), rabbit anti-p19INK4d (M-167, Santa Cruz Biotechnology), rabbit anti-CDK5 (C-8, Santa Cruz Biotechnology), rabbit anti-CDK2 (M2, Santa Cruz Biotechnology), rabbit anti-p35 (C-19, Santa Cruz Biotechnology), mouse anti-β-actin (C4, Santa Cruz Biotechnology), mouse anti-V5 (R960-25, Invitrogen), rabbit anti-MAP2 (Cell Signaling Technology), mouse anti-phospho-H2A.X (Ser139) (JBW301, Upstate), mouse anti-phospho-ATM (Ser1981) (10H11.E12, Abcam), and rabbit anti-ATM (Abcam). Anti-mouse and anti-rabbit secondary antibodies conjugated with horseradish peroxidase were purchased from Sigma (Saint Louis, USA).

2.5. Metabolic labeling and immunoprecipitation of phospho-p19

Differentiated SH-SY5Y cells were grown in 60-mm dishes. Cells were incubated with 0.5 mCi [^{32}P]-sodium orthophosphate for 3 h prior to their treatment as indicated in each experiment. At different time points after treatments, cells were washed, collected in cold PBS and lysed in RIPA buffer. The lysates (100 μg) were incubated with polyclonal rabbit p19 antibody (M-167, Santa Cruz Biotechnology) for 2 h, followed by an overnight incubation with protein A/G agarose beads (Santa Cruz Biotechnology) at 4 °C. After washing three times with PBS, samples were analyzed by SDS-PAGE. Dried gels were exposed to a radiographic intensifying screen by Fujifilm and scanned directly using a Bio-Imaging Analyzer Fujifilm BAS-1800II.

2.6. CDK5 in vitro kinase assay

In vitro kinase assay was performed as described before [34]. Briefly, differentiated SH-SY5Y cells were washed with PBS and lysed in HB buffer (25 mM MOPS pH 7.2, 15 mM EGTA, 15 mM $MgCl_2$, 1 mM DTT, 1% Tritón-X 100, 0.5 mM NaF, 0.1 mM sodium orthovanadate, 1 mM PMSF, 1× protease inhibitor cocktail). Proteins (0.5 mg) were immunoprecipitated with 1 μg of anti-CDK5 antibody (C-8, sc-173, Santa Cruz Biotechnology) and 20 μl of 50% slurry of protein A/G-agarose beads (Sigma) and rocked at 4 °C for 2 h. For the control sample containing only the substrate (histone H1 derived peptide, p-H1, PKTPKKAKKL) but no enzyme, proteins were incubated with the beads without anti-CDK5 antibody. The beads were washed and resuspended in a 15 μl HB buffer. Each sample was added 15 μl of 2× kinase reaction buffer (HB buffer containing 200 μM ATP, 200 μM p-H1 and 1 μl of [γ-^{32}P] ATP (6000 Ci/mmol [10 μCi/μl]) per 10 μl of 2× reaction buffer). Samples were incubated for 30 min at 37 °C. Following the reaction, samples were processed according to the phosphocellulose paper method. As a negative control, the reaction was conducted without substrate. In a similar assay, phosphorylation of a p19 derived peptide containing the surrounding sequence of S76 (p-S76; RGTSPVHDAART; 200 mM) was tested. As control for CDK5 activity, the histone H1 derived peptide was used. As a negative control, the reaction was conducted without substrate (none).

To evaluate the direct phosphorylation of p19 by CDK5, differentiated SH-SY5Y cells were lysed in HB buffer. Proteins (1 mg) were immunoprecipitated with 2 μg of anti-CDK5 antibody and 50 μl of 50% slurry of protein A/G-agarose beads (SIGMA) and rocked at 4 °C for 2 h. For the control sample containing only the substrate (GST-p19) but no enzyme, proteins were incubated with the beads without anti-CDK5 antibody. The beads were washed and resuspended in a 15 μl HB buffer. Each sample was added 15 μl of 2× kinase reaction buffer (HB buffer containing 200 μM ATP, 1 mg/ml GST-p19, and 1 μl of [γ-^{32}P]ATP (6,000 Ci/mmol [10 μCi/μl]) per 10 μl of 2× reaction buffer). Samples were incubated for 20 min at 37 °C. The reaction was stopped by an addition of 7.5 μl of 5× sample buffer and 5 min incubation at 95 °C. Histone H1 from calf thymus (Calbiochem) was used for kinase activity control. Samples were electrophoresed on 12% denaturing gels. Gels were dried on Whatman paper, exposed to a radiographic intensifying screen by Fujifilm and scanned directly using a Bio-Imaging Analyzer Fujifilm BAS-1800II.

2.7. Unscheduled DNA synthesis

SH-SY5Yempty, SH-SY5Yp19S and SH-SY5Yp19AS cells were seeded at 1×10^6 cells per 35-mm plate and treated with 1 μM ATRA during 6 days. After differentiation, cells were incubated with a culture medium containing 0.5% fetal bovine serum and 100 μM $ZnSO_4$. We determined that under these conditions, DNA semi-conservative synthesis was completely inhibited. After 16 h, the medium was changed to a fresh medium containing 1% fetal calf serum and incubated with 10 μM β-amyloid peptide or 100 ng/ml NCS and 10 μCi/ml [^{3}H]-thymidine. Hippocampal neurons were seeded at 5×10^5 cells per 35-mm plate. After 2 days, neurons were transfected with p19 antisense oligonucleotide and, 24 h later, incubated with 10 μM β-amyloid peptide or 50 ng/ml NCS and 10 μCi/ml [^{3}H]-thymidine. At the indicated times, SH-SY5Y or neuron cells were washed three times with cold PBS, harvested and pelleted at 3000 ×*g* for 5 min. The cells were lysed with 5% TCA for 30 min and centrifuged at 10000 ×*g* for 10 min. The pellet was washed twice with cold PBS and resuspended in 1 M NaOH. The incorporated radioactivity was quantified by scintillation counting. Unscheduled DNA synthesis was estimated as dpm/μg of protein.

2.8. Caspase-3 activity

SH-SY5Yempty, SH-SY5Yp19S and SH-SY5Yp19AS cells were seeded at 1×10^6 cells per 35-mm plate and treated with 1 μM ATRA during six days. After differentiation, cells were incubated with 100 μM $ZnSO_4$ for 16 h and, then, incubated with 10 μM β-amyloid peptide or 100 ng/ml NCS. Hippocampal neurons were seeded at 5×10^5 cells per 35-mm plate. After 2 days, neurons were transfected with p19 antisense oligonucleotide and, 24 h later, incubated with 10 μM β-amyloid peptide or 100 ng/ml NCS. Twenty-four hours after genotoxic treatment caspase-3 activity was determined as previously described [34]. Caspase activity was estimated at A_{405}/μg protein.

2.9. Cell viability assay

Cell viability was assessed by 3-[4,5-dimethylthiazol-2-yl]-2,5-diphenyltetrazolium bromide (MTT) assay. Exponentially growing SH-SY5Yp19S or SH-SY5Yp19AS cell lines (1×10^5 cells/well) were seeded in 24-well plates and incubated with 100 μM $ZnSO_4$ for 16 h. Then, cells were incubated with 50 ng/ml NCS. At the indicated times, the culture media were replaced by 1 ml of fresh medium containing MTT

(Sigma) to a final concentration of 0.5 mg/ml and incubated at 37 °C. After 4 h incubation, the medium and MTT were removed and 500 μl of isopropanol was added. Plates were shaken for 15 min and the absorbance in the solvent was determined at 570 nm. The background was subtracted by using a dual-wavelength setting of 570 and 650 nm. Control included untreated cells and medium alone. Hippocampal neurons (4×10^4 cells/well) were seeded in 96-well plates. After two days, neurons were transfected with p19 antisense oligonucleotide and, 24 h later, incubated with 10 μM β-amyloid peptide or 50 ng/ml NCS and cell viability was determined as described above.

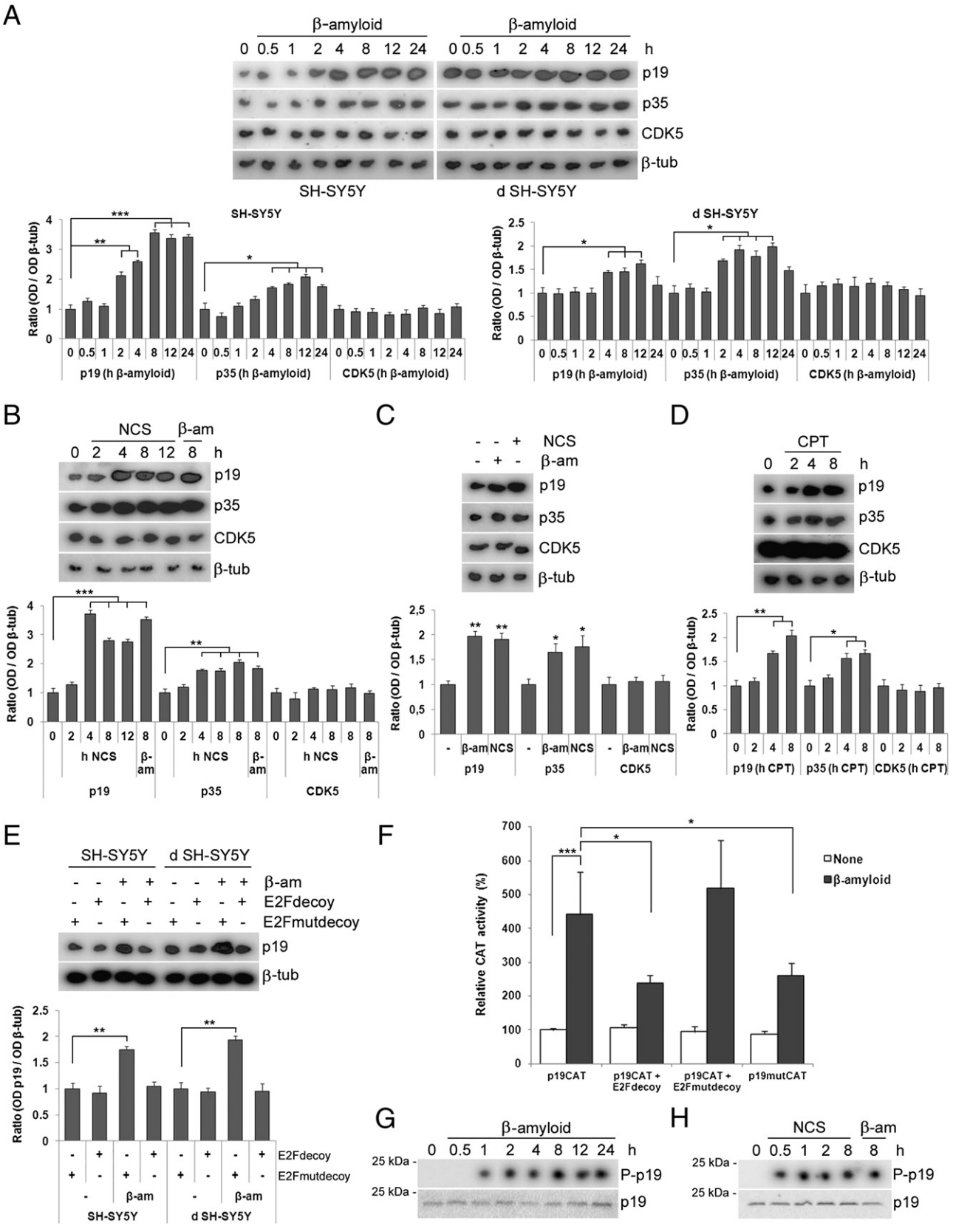

2.10. Clonogenic assay

Survival after NCS treatment was determined by clonogenic assay in SH-SY5Yp19AS clonal cells. Cells were plated as single cell and treated with different doses of NCS after metallothionein promoter induction with 100 μM $ZnSO_4$ for 16 h. Cells were incubated for 15 days followed by fixation with 10% formaldehyde, staining by the addition of crystal violet (5 mg/ml in ethanol) and surviving clones counted. Colonies containing >50 cells were rated as deriving from viable, clonogenically capable cells.

2.11. Animals

Wistar female rats were provided by the Bioterio Central Facultad de Ciencias Exactas y Naturales, University of Buenos Aires. C57BL/6J male mice, 60–70 d of age, weighting 25–30 g, were used (La Plata University Animal Facilities, La Plata, Argentina). The animals were individually caged and singly housed throughout the experimental procedures, with water and food ad libitum, under a 12 h light/dark cycle (lights on at 8:00 A.M.) at temperature of 21–22 °C. Experiments were performed in accordance with local regulations and the National Institutes of Health (NIH) *Guide of the Care and Use of Laboratory Animals* (NIH Publication 80-23/96) and were previously approved by the Ethical Committee of the Facultad de Ciencias Exactas y Naturales, University of Buenos Aires. All efforts were made to minimize animal suffering and to reduce the number of animals used.

2.12. Surgery and injections

Mice were implanted under deep anesthesia (ketamine and xylazine) with a 23-G guide cannula 1 mm dorsally to the dorsal hippocampus, at coordinates A −1.9, L ± 1.2, V 1.2 in accordance with the atlas of Franklin and Paxinos [35]. Guide cannulae were fixed to the skull with dental acrylic. Experiments were performed following animal recovery and injections were administered without anesthesia. The injection device consisted of a 30-G cannula connected to a 5 μl Hamilton syringe with tubing. Initially, the infusion device was filled with distilled water and a small air bubble was sucked into the injection cannula, followed by the injection solution. The air bubble allowed for a visual inspection of the injection progress. The injection cannula was inserted into the guide cannula with its tip extending beyond the guide by 1 mm in order to reach the dorsal hippocampus. The injections were administered during 30 s, and operated by hand. The injection cannula was removed after 60 s in order to avoid reflux and to allow the diffusion of drugs. The volume of each intrahippocampal infusion was 0.5 μl. Different injection devices were used for drug and vehicle. Only data from animals with cannulae located in the intended sites were included in the analysis.

p19 antisense oligodeoxynucleotide (ODN) and its scrambled sequence were injected at 1 nmol/μl in all antisense experiments. Sequences: p19 antisense (p19ASODN: 5′-AGAAGCATAGTGGATACCGG-3′) and p19 scrambled (ScrODN: 5′-ACAAGTTGGACACGGGAGAT-3′). Vehicle: Hank's balanced salt solution (HBSS, pH 7.4). The antisense for p19 mRNA was specific for the sequence that includes the translational start side. The respective ScrODN, which served as control, contained the same base composition but in random order and show no homology to sequences in the GenBank database. All oligonucleotides were phosphorothiolated on the three terminal bases both 5′ and 3′ ends to produce increased stability [36]. NCS (Sigma-Aldrich) was dissolved in HBSS and administrated at a final concentration of 25 ng/ml, except for the dose–response curve (10, 25 and 100 ng/ml). ODNs injections were done 16 h before NCS injection.

2.13. Immunohistochemistry

At the indicated times after NCS injections, mice were anesthetized and perfused with 4% paraformaldehyde in PBS. Their brains were postfixed overnight in the same fixative with 30% sucrose. Sixty-micrometer coronal sections were cut through the hippocampus in a vibrating microtome. Sections were stored in a cryoprotectant solution (25% glycerol, 25% ethylene glycol, 50% phosphate buffer 0.1 M pH 7.4) at −20 °C until use. Immunohistochemistry technique was performed on free-floating sections from 4 mice per group. Sections were blocked for 1 h in PBS with 0.3% Triton X-100 and 5% goat serum and incubated for 48 h at 4 °C in a clinical rotator with a mouse monoclonal anti-phospho-H2AX (Ser 139) antibody (1:200; JBW301, Upstate) diluted in a blocking solution. After incubation with secondary fluorescent antibody (anti-mouse Alexa 594, 1:1000; Invitrogen), sections were mounted with DAPI-Fluoromount-G (SouthernBiotech). Slides were visualized using an Eclipse E600W Nikon microscope and images were acquired with a Coolpix 5000 Nikon digital camera. Quantification of γH2AX-positive cells were performed using ImageJ software (NIH).

2.14. Y-maze test

Working memory performance was assessed by recording continuous alternation behavior during a single session in a Y-maze device. The maze was made of transparent acrylic. Each arm was 40 cm long, 13 cm high, 3 cm wide at the bottom, 10 cm wide at the top, and converging at an equal angle. Each mouse was placed at the end of one arm and allowed to move freely through the maze during a 10-min session. The series of arm entries was recorded using the ANY-maze software via a camera mounted directly about the maze. A correct alternation was defined as entries into all three arms on consecutive occasions. The number of maximum alternations was therefore the total

Fig. 1. β-Amyloid peptide and neocarzinostatin treatments trigger the induction of mRNA p19 and the phosphorylation of its protein in neuronal cells. (A) SH-SY5Y cells (left panel) and differentiated SH-SY5Y cells (right panel) were incubated with 10 μM β-amyloid peptide. Total RNA (10 μg) extracted from cells at the indicated times were subjected to Northern blot analysis with the ^{32}P-labeled probes specified at the right margin. (B) Differentiated SH-SY5Y cells were treated with 100 ng/ml neocarzinostatin or 10 μM β-amyloid peptide as indicated. At different time points, the expression of p19, p35 and CDK5 were assessed by Northern blot. (C and D) Cultured hippocampal neurons were incubated with 100 ng/ml neocarzinostatin or 10 μM β-amyloid peptide (C) or 1 μM camptothecin (D). After 4 h (C) or at the indicated times (D), total RNA was extracted from neurons and subjected to Northern blot analysis. (A–D) The figure shows a representative autoradiograph of three independent experiments with similar results. Densitometric analysis of p19, p35 and CDK5 are represented in the lower panels. Bars represent the mean ± S.D. of three experiments. Student's *t*-test was used to compare samples obtained at different times with samples obtained at zero time (*$p < 0.05$; **$p < 0.02$; ***$p < 0.01$). (E) SH-SY5Y cells (left panel) and differentiated SH-SY5Y cells (right panel) were transfected with wild-type or mutant E2F decoy. After 24 h cells were treated with 10 μM β-amyloid peptide for additional 4 h. Cells were harvested and subjected to Northern blot analysis using a ^{32}P-labeled probe specific for human p19 mRNA and reprobed for β-tubulin mRNA. The figure shows a representative autoradiograph of three independent experiments with similar results. Densitometric analysis of p19 is represented in the lower panel. Bars represent the mean ± S.D. of three experiments. Student's *t*-test was used to compare each sample with mutant E2F decoy transfected and none treated samples (**$p < 0.02$). (F) Differentiated SH-SY5Y cells were transiently cotransfected with 4 μg p19CAT or equivalent amount of mutant plasmid (p19mutCAT), 4 μg pCEFL-β-galactosidase and 250 nM wild-type or mutated E2F decoy, as indicated. After 24 h, cells were treated or not with 10 μM β-amyloid peptide. CAT activity was determined 24 h after β-amyloid treatment and normalized to β-galactosidase activity. Results are expressed as relative CAT activity with respect to basal value of p19CAT which was set to 100. Bars represent the mean ± S.D. of three independent experiments performed in quadruplicate. Student's *t*-test was used to analyze data as indicated (*$p < 0.05$; ***$p < 0.01$). (G and H) Differentiated SH-SY5Y cells were labeled with [^{32}P]-orthophosphate and treated with 10 μM β-amyloid peptide (G) or 100 ng/ml neocarzinostatin (H) for the indicated times. Equal amounts of whole cell extracts were subjected to immunoprecipitation with anti-p19 antibody and the immune complexes were analyzed by SDS-PAGE and autoradiography (upper panels; P-p19, phosphorylated p19) or immunoblotting (lower panels; p19). The figure shows a representative autoradiograph of tree independent experiment with similar results. β-Amyloid peptide (β-am), neocarzinostatin (NCS), β-tubulin (β-tub), camptothecin (CPT), decoy E2F oligonucleotide (E2Fdecoy), mutated decoy E2F oligonucleotide (E2Fmutdecoy), and optic densitometry (OD).

number of arm entries minus two, and the percentage of alternation was calculated as [correct alternations / maximum alternations] × 100.

Spatial learning was evaluated using a two-trial recognition memory test with the Y-maze [37]. The walls of the arms were transparent allowing the mouse to see distal spatial landmarks. The inside of the arms was identical providing no intramaze cues. Mice were placed into one of the arms of the maze (start arm) and allowed to explore the maze with one of the arms closed for 15 min (training trial). After a 30 min intertrial interval, mice were returned to the Y-maze by placing them in the start arm and allowed to explore freely all three arms of the maze for 5 min (test trial). The number of entries into and the time spent in each arm, and the first choice of entry were registered from video recordings.

2.15. Fear conditioning test

The conditioning chamber was made of transparent acrylic (24.5 × 24.5 × 42 cm) in a wooden box with a clear front lid. The floor of the chamber consisted of parallel stainless steel grid bars, each measuring 0.3 mm diameter and spaced 0.8 mm apart. The grid was connected to a device to deliver the foot-shocks and tone presentations. Before training, the animals were handled once a day for two days. Training (day 1) consisted of placing the mouse in the chamber and allowing a 2 min acclimatization period. After this period, the mouse received three trials (with an intertrial interval of 1 min) of a tone presentation (10 s, 80 dB) which co-terminated with a foot-shock (0.6 mA, 1 s). After the final trial, the mouse remained in the chamber for an additional minute and was returned to its home cage. Contextual fear conditioning during the test session was evaluated one day after training (day 2) by placing each mouse in the training environment for 5 min in the absence of the foot-shock and the tone. Animals were also tested to the tone (cued fear conditioning) one day after the contextual test (day 3). This test was performed by presenting the same tone used in the training session, but in a modified context. Most of the contextual cues present in the training context were changed (white floor, semicircular green walls, vanilla odor, different chamber and room light intensity, and absence of background noise). The tone was presented for 4 min after a baseline period of 2 min to evaluate pre-tone freezing. Training, contextual and cued tests were videotaped to calculate freezing.

Memory was assessed and expressed as the percentage of time that the mice spent freezing, which is commonly used as an index of fear in mice [38]. Freezing was defined as the absence of movements except those related to breathing, and was scored according to an instantaneous time-sampling procedure, in which each animal was observed every 5 s (60 measures for the contextual memory test; and 72 measures for the cue memory test: 24 measures for the pretone and 48 measures for the tone).

2.16. Data analyses

Data were analyzed by unpaired two-tailed Student's *t* test. Quantification of γH2AX immunofluorescence in hippocampus, spontaneous alternation Y-maze test and contextual fear conditioning test were statistically analyzed by one-way ANOVA, followed by Bonferroni's post hoc test. When cued fear memory was assessed, behavioral data were analyzed by two-way ANOVA, followed by Bonferroni's post hoc test. Cued Y-maze test was analyzed using chi-square test.

3. Results

3.1. p19 is induced and phosphorylated in neuronal cells in response to DNA damage

In a first approach in order to contrast our hypothesis about the role of p19 in the cellular response evoked by genotoxic-induced DNA damage, we analyzed the expression of p19 in differentiated cells treated with β-amyloid peptide. To do this, human neuroblastoma SH-SY5Y cells were incubated with 1 μM all-*trans*-retinoic acid (ATRA) for seven days. The emergence of long and interconnected neurites, the expression of microtubule-associated protein 2 from the third day of incubation and the diminished expression of CDK2 indicate that cells were differentiated to neuronal-type cells (Supplementary Fig. 1A–D).

Time-course experiments revealed that p19 mRNA expression was early and significantly induced upon treatment with 10 μM β-amyloid in both differentiated and non-differentiated SH-SY5Y cells (Fig. 1A). Similar results were observed in differentiated cells treated with 100 ng/ml neocarzinostatin (NCS) (Fig. 1B), a radiomimetic drug that generates DNA-double strand beaks (Supplementary Fig. 1E and Supplementary Fig. 4D). Induction of p19 expression was also detected in the primary culture of rat hippocampal neurons incubated with NCS or β-amyloid peptide (Fig. 1C) or 1 μM camptothecin (Fig. 1D). This induction appears to be attributable to transcriptional regulation and mediated by E2F transcription factor since SH-SY5Y cells transfected with the decoy oligodeoxynucleotide containing a wild type version of the E2F consensus binding sequence and treated with β-amyloid, showed lower p19 induction than cells transfected with the decoy containing a mutated version of the E2F binding site (Fig. 1E). Similarly, the β-amyloid-mediated induction of a reporter construct harboring a 2307-bp fragment derived from the human p19 promoter was partially repressed in cells co-transfected with the wild type decoy but not in those co-transfected with the mutated version or when the two E2F binding sites in the p19 promoter were mutated (Fig. 1F).

p19 not only showed increased expression, but was also phosphorylated by incubation of differentiated SH-SY5Y cells with β-amyloid peptide or NCS (Fig. 1G and H), as we had observed in non-neuronal cells under stress conditions [34]. p19 phosphorylation was detectable within 30–60 min and maintained for at least 24 h after β-amyloid treatment or 8 h after incubation with NCS.

Interestingly, p19 mRNA and protein levels were increased during the differentiation process with ATRA (Supplementary Fig. 2A and B). p19 protein was four or five times higher in neuronal-type cells than in non-differentiated cells and remained increased along the experimental period. This induction in p19 expression could be due to the action of the transcription factor Egr-1, which was induced during differentiation itself (Supplementary Fig. 2A). Besides the presence of several putative Egr-1 binding sites on the p19 promoter, two experimental evidences strongly support this hypothesis. First, overexpression of Egr-1 induced p19 expression in SH-SY5Y cells in the absence of any differentiation stimulus. Second, in ATRA-stimulated SH-SY5Y cells previously incubated with an Egr-1 antisense oligodeoxynucleotide, p19 induction was almost completely blocked although the differentiation process progressed without changes (Supplementary Fig. 2C–E).

The following experiments, unless otherwise mentioned, were carried out in SH-SY5Y differentiated cells.

3.2. p19 phosphorylation depends on CDK5 activity

Recently, we have demonstrated that CDK2 phosphorylates p19 in serine 76 upon UV-induced DNA damage [34]. This serine is located in a consensus motif for CDK1/CDK2/CDK5 phosphorylation. In view of the high activity of CDK5 in neuronal cells, we next attempted to find out whether p19 is a physiologically relevant target of this kinase under DNA damage conditions. In agreement with previous reports [39,40], we found that β-amyloid induced a sustained activation of CDK5 (Fig. 2A). Surprisingly, NCS promoted an increase in CDK5 activity as well (Fig. 2A). As expected, enhancement of CDK5 kinase activity by NCS promoted phosphorylation of ATM, a CDK5 substrate [41] (Fig. 2B). As the kinase activity of CDK5 is dependent on its activator p35, we next examined the levels of p35 and CDK5 transcripts. The levels of p35 mRNA, but not of CDK5, increased within 2 h after β-amyloid or NCS incubation in both SH-SY5Y differentiated cells (Fig. 1A and B) and

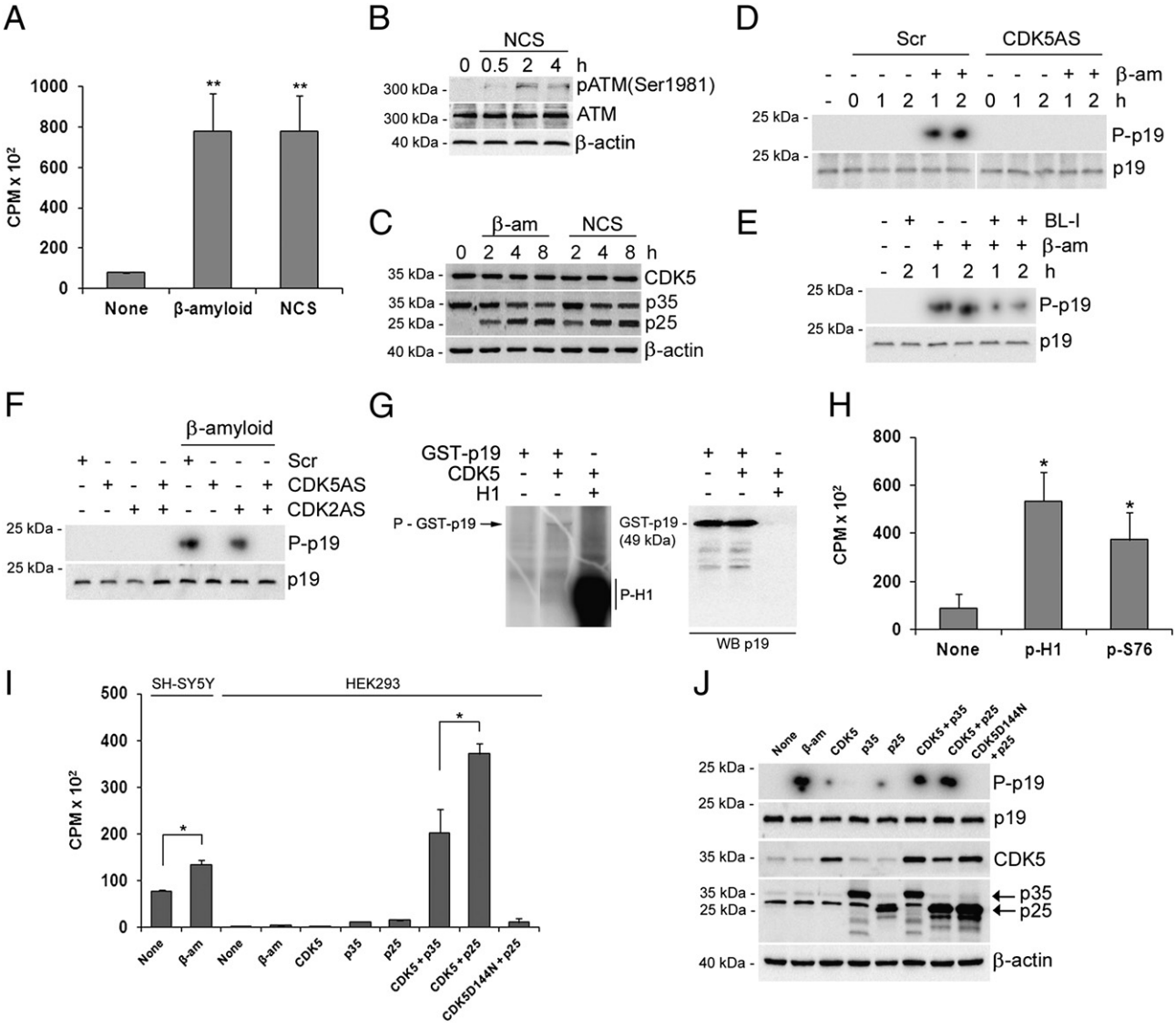

Fig. 2. p19 phosphorylation depends on CDK5 activity in damaged neuronal type cells. (A) In vitro kinase assays were performed using immunoprecipitated CDK5 from differentiated SH-SY5Y cells previously treated or not with 10 μM β-amyloid peptide or 100 ng/ml neocarzinostatin. Histone H1 derived peptide was used as a specific substrate to measure kinase activity. Measurements were done in triplicates and bars show the mean ± S.D. of three independent experiments. Student's *t*-test was used to compare treated and non-treated samples (**$p < 0.02$). (B) Differentiated SH-SY5Y cells were treated with 100 ng/ml neocarzinostatin during 0.5, 2 and 4 h. Whole-cell extracts were prepared and analyzed by Western blotting for phosphoATM (s1981), ATM and β-actin. The figure is a representative of three independent experiments with similar results. (C) Differentiated SH-SY5Y cells were treated with 10 μM β-amyloid or 100 ng/ml neocarzinostatin and harvested at different time points. Cultured hippocampal neurons were incubated with 10 μM β-amyloid peptide or 100 ng/ml NCS and harvested 4 h after treatments. The expression of CDK5, p35 and p25 were evaluated by Western blot using specific antibodies. The figure is a representative of three independent experiments with similar results. (D) Differentiated SH-SY5Y cells were transfected with an antisense oligodeoxynucleotide to CDK5 (CDK5AS) or its scrambled version (Scr). After 24 h, cells were labeled with [^{32}P]-orthophosphate for 3 h and then treated with 10 μM β-amyloid peptide. (E) Differentiated SH-SY5Y cells were labeled with [^{32}P]-orthophosphate for 3 h, pre-treated with 10 μM butyrolactone-I for another 2 h and then damaged with 10 μM β-amyloid peptide. (D and E) At the indicated time points, endogenous p19 phosphorylation was analyzed by SDS-PAGE and autoradiography (upper panels; P-p19, phosphorylated p19) or immunoblotting (lower panels; p19). The figure shows a representative autoradiograph of three independent experiments with similar results. (F) Differentiated SH-SY5Y cells were transfected with an antisense oligodeoxynucleotide to CDK5 (CDK5AS) or to CDK2 (CDK2AS) or their respective scrambled sequence (Scr). After 24 h, cells were labeled with [^{32}P]-orthophosphate for 3 h and then treated with 10 μM β-amyloid peptide for 2 h. Endogenous p19 phosphorylation was analyzed by SDS-PAGE and autoradiography. The figure shows a representative autoradiograph of three independent experiments with similar results. (G) In vitro kinase assays were performed using immunoprecipitated CDK5 from β-amyloid-damaged SH-SY5Y cells and recombinant GST-p19. Histone H1 was used as a control for CDK5 activity. The control lane 1 belongs to the same gel (left panel). Aliquots of each sample were electrophoresed and the presence of GST-p19 was analyzed by Western blot using an anti-p19 monoclonal antibody (right panel). The figure shows a representative autoradiograph of three independent experiments with similar results. (H) A synthetic peptide containing the sequence in which S76 (p-S76) is positioned, was used to perform in vitro kinase assays. p-S76 peptide was incubated with CDK5 immunoprecipitated from β-amyloid-damaged SH-SY5Y cells. A histone H1 peptide (p-H1) was used as a specific substrate for CDK5 as a control of enzymatic activity. Measurements were done in triplicates and bars show the mean ± S.D. of three independent experiments. Student's *t*-test was used to compare substrates containing samples with samples without substrate (none) (*$p < 0.05$). (I and J) HEK293 cells were cotransfected with CDK5, p35, p25 or CDK5D144N expression vectors along with pBabe-Puro. Twenty-four h after transfection cells were treated with 1 μg/ml puromycin and incubated for another 48 h. In (I), differentiated SH-SY5Y cells and resistant HEK293 cells were damaged with 10 μM β-amyloid peptide for 2 h and cell extracts were used to perform in vitro CDK5 kinase assay. Measurements were done in triplicates and bars show the mean ± S.D. of three independent experiments. Student's *t*-test was used to compare treated vs. non-treated SH-SY5Y cells and CDK5 + p35 vs. CDK5 + p25 transfected HEK293 cells (*$p < 0.05$). In (J) puromycin resistant cells were labeled with [^{32}P]-orthophosphate for 3 h, treated with 10 μM β-amyloid peptide and collected 2 h after damage. Extracts were subjected to immunoprecipitation with antip19 antibody and phosphorylated p19 (P-p19) was analyzed by autoradiography. The levels of endogenous p19 and transfected CDK5 and p35/p25 were also controlled by Western blot. The figure shows a representative autoradiograph of three independent experiments with similar results. β-Amyloid peptide (β-am), neocarzinostatin (NCS), and butyrolactone-I (BL-I).

hippocampal neurons (Fig. 1C). In addition, induction of p35 cleavage to p25 by β-amyloid or NCS was observed in both SH-SY5Y differentiated cells and hippocampal neurons (Fig. 2C). These results indicate that expression and proteolysis of p35 are strongly induced by these genotoxics and that kinase activity of CDK5 is thereby greatly enhanced.

To determine whether increased CDK5 activity is required for β-amyloid-mediated induction of p19 phosphorylation, cells were either previously transfected with a CDK5 antisense oligodeoxynucleotide or treated with butyrolactone-I, a CDK5 inhibitor, to decrease this kinase activity (Supplementary Fig. 3A and B). We found that the antisense oligodeoxynucleotide totally inhibited while butyrolactone promoted a significant decrease in p19 phosphorylation (Fig. 2D and E). Unlike non-neuronal cells, in which the genotoxic triggers CDK2-dependent p19 phosphorylation [34], postmitotic neurons appear to activate CDK5 to target p19 under a stress stimulus, as suggested by the results shown in Fig. 2F. The CDK5, but not the CDK2 antisense oligonucleotide to CDK5, was able to suppress the p19 phosphorylation induced by incubation with β-amyloid peptide (Fig. 2F and Supplementary Fig. 3C–E). On the other hand, induction of p19 expression seemed to be independent of CDK5 (Supplementary Fig. 3F and G).

To investigate whether p19 is a direct target of CDK5 we carried out in vitro kinase assays using recombinant GST-p19 protein or specific p19 derived peptide containing serine 76 as substrates with CDK5 immunoprecipitated from SH-SY5Y cells. The results showed that CDK5 was able to efficiently phosphorylate both the purified GST-p19 and the S76-containing peptide (Fig. 2G and H). These results indicate that p19 is a proper substrate for the CDK5 activity. It is important to note that we have previously demonstrated that mutation in S76 render a non-phosphorylatable p19 protein [34].

To further examine the requirement for CDK5 activity, we carried out p19 phosphorylation assays in non-neuronal cells lacking endogenous p35 expression. HEK293 cells were transfected with an expression vector encoding CDK5, and/or p35 and/or p25 to reconstitute CDK5 activity in these cells (Fig. 2I). Incubation with a β-amyloid peptide phosphorylated p19 in HEK293 cells probably through activation of

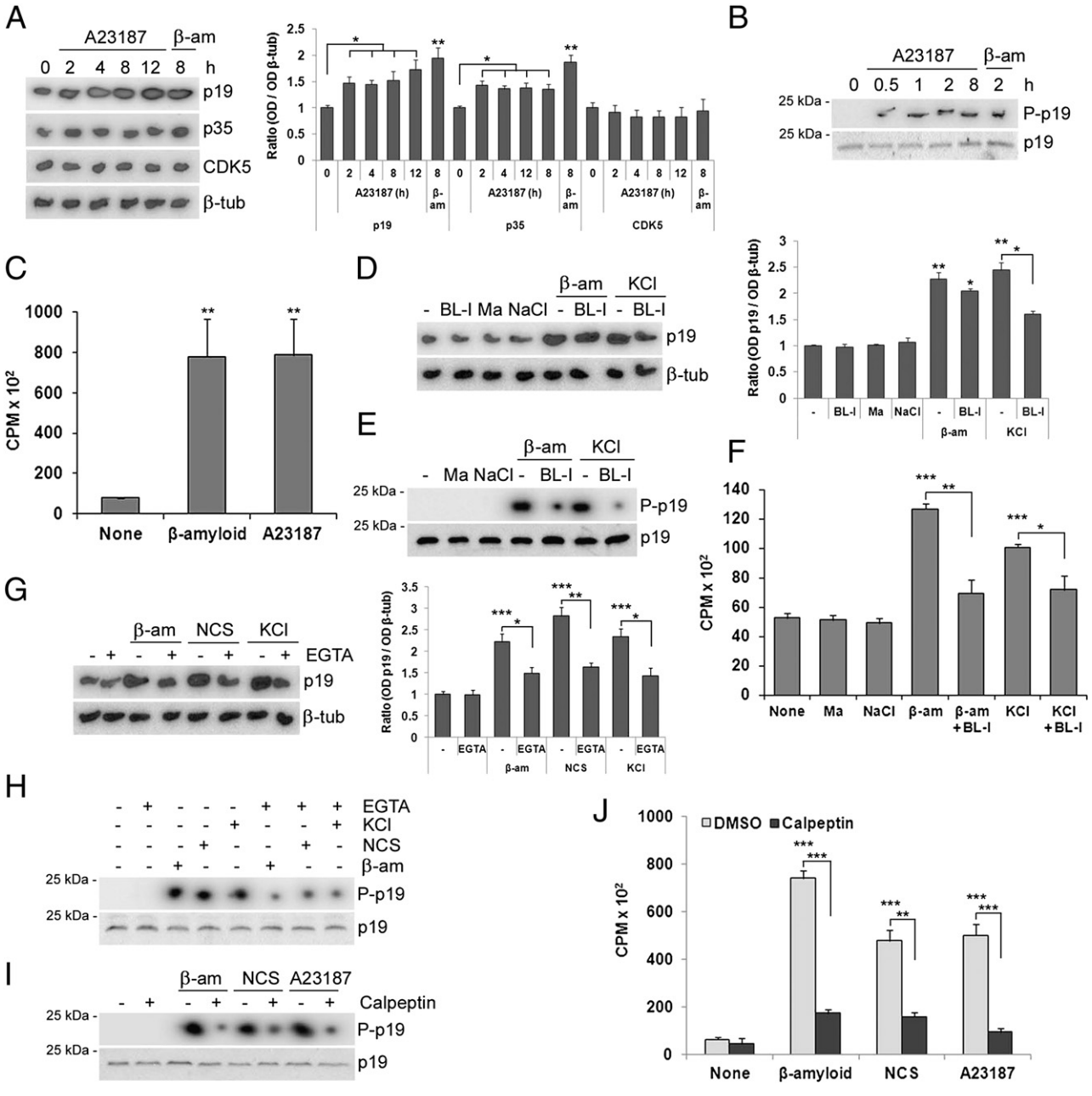

CDK2, as previously reported [34]. However, only overexpression of CDK5/p35 or CDK5/p25 led to a robust p19 phosphorylation in the absence of genotoxic stimuli (Fig. 2J). Overexpression of a dominant negative form of CDK5 with p25 alone severely impaired CDK5 activity and p19 phosphorylation was no longer observed.

Together these results indicate that increased CDK5 activity, in response to β-amyloid or NCS, is required for p19 phosphorylation in neuronal-type cells.

3.3. An increase in intracellular calcium recapitulates the DNA damage-mediated effect on p19 expression

It is known that β-amyloid-mediated activation of CDK5 caused by the stimulation of the proteolytic activity of calpain over p35 rendered the more potent CDK5 regulatory subunit, p25. Calpain activity is increased in response to the increased influx of calcium ions in neuronal cells promoted by incubation with β-amyloid. In view of this, we asked whether increasing intracellular levels of calcium, in the absence of genotoxics, would be sufficient to modify p19 expression and phosphorylation. To test this, differentiated SH-SY5Y cells were incubated with the calcium ionophore A23187. We found that p19 expression and phosphorylation were increased in response to the calcium ionophore to levels comparable to those observed in the presence of β-amyloid peptide (Fig. 3A–C).

To further assess the role of calcium, differentiated cells were incubated with a medium containing ten times higher potassium concentration to trigger membrane depolarization and increase the levels of intracellular calcium. Like that observed after incubation with the ionophore, p19 expression and phosphorylation were increased after membrane depolarization. Again, p19 phosphorylation was dependent on CDK5 activity as it was inhibited by incubation with butyrolactone (Fig. 3D–F). Interestingly, in this case, p19 induction was also dependent on CDK5 activity. These observations were not a mere effect of an increased saline concentration or osmolarity of the cell incubation medium because a similar concentration of NaCl or mannose addition caused no changes in p19 mRNA expression or p19 phosphorylation (Fig. 3D–F). To confirm that these effects were dependent on the increased levels of intracellular calcium, we incubated cells in each of the above conditions in the presence of EGTA to quelate calcium ions. Both the induction and phosphorylation of p19 mediated by β-amyloid, NCS or high potassium concentration were severely impaired in the presence of EGTA (Fig. 3G and H).

As already mentioned, DNA damage in neuronal cells promotes and increases CDK5 activity mainly caused by the calpain-mediated cleavage of p35 to p25. Then, we tested whether p19 phosphorylation in response to DNA damage or increased calcium levels is dependent on calpain proteolytic activity. Differentiated SH-SY5Y cells were cotreated with β-amyloid, NCS or A23187 ionophore and the calpain inhibitor calpeptin. We found that calpeptin partially inhibited the p19 phosphorylation (Fig. 3I). As expected, the induction of CDK5 activity promoted by incubation with the genotoxics or the ionophore was blocked by calpeptin (Fig. 3J).

3.4. CDK5-mediated phosphorylation stabilizes p19 protein

In a previous work we have demonstrated that UV irradiation of a great number of different cells leads to p19 induction of both mRNA and protein expression ([25] and Supplementary Fig. 4A). However, in spite of the increase in p19 mRNA expression in response to β-amyloid or NCS treatment, we found no significant increase in p19 protein levels in neuronal cells (Fig. 4A). Similar results were obtained in Neu-2a cells and primary cultures of rat hippocampal neurons (Supplementary Fig. 4B–D).

Consistent with a previous report [42], we found that p19 protein is degraded by calpain protease (data not shown). Therefore, the same mechanism leading to CDK5 activation in response to intracellular calcium influx and mediating induction of p19 expression and phosphorylation, could be involved in p19 partial degradation. To test the above hypothesis, we determined the effect of β-amyloid peptide on p19 protein expression in the presence of the calpain inhibitor, calpeptin. We found increased levels of p19 protein when cells were coincubated with β-amyloid and calpeptin (Fig. 4B). Similar results were obtained in differentiated SH-SY5Y cells incubated with NCS along with calpeptin (Fig. 4C). Thus, these results indicate that p19 is subjected to calpain degradation activated by increased intracellular calcium levels.

Next, we asked whether p19 phosphorylation could be related to its degradation upon calpain activation. When differentiated SH-SY5Y cells were preincubated with a CDK5 antisense oligodeoxynucleotide or with the CDK5 inhibitor butyrolactone and then treated with β-amyloid peptide, p19 protein levels were lower than those in cells preincubated with the scrambled oligodeoxynucleotide or vehicle alone (Fig. 4D and E). To further confirm the function of phosphorylation on p19 stability, we conducted experiments in differentiated SH-SY5Y cells

Fig. 3. Increased levels of intracellular calcium cause the induction and phosphorylation of p19. (A) Differentiated SH-SY5Y cells were incubated with 5 μM A23187 or 10 μM β-amyloid peptide and harvested at the indicated times following treatment. Total RNA (10 μg) was extracted from cells and subjected to Northern blot analysis using the [^{32}P]-labeled probes specified at the right margin. The figure is representative of three independent experiments with similar results. Densitometric analysis of p19, p35 and CDK5 are represented in the right panel. Bars represent the mean ± S.D. of three experiments. Student's *t*-test was used to compare samples obtained at different times with samples obtained at zero time (*$p < 0.05$; **$p < 0.02$). (B) Differentiated SH-SY5Y cells were labeled with [^{32}P]-orthophosphate and treated with 5 μM A23187 or 10 μM β-amyloid peptide for the indicated times. Equal amounts of whole cell extracts were subjected to immunoprecipitation with anti-p19 antibody and the immune complexes were analyzed by SDS-PAGE and autoradiography (upper panels; P-p19, phosphorylated p19) or immunoblotting (lower panels; p19). The figure shows a representative autoradiograph of three independent experiments with similar results. (C) In vitro kinase assays were performed using immunoprecipitated CDK5 from differentiated SH-SY5Y cells previously treated with 10 μM β-amyloid peptide or 5 μM A23187. Histone H1 derived peptide was used as a specific substrate to measure kinase activity. Measurements were done in triplicates and bars show the mean ± S.D. of three independent experiments. Student's *t*-test was used to compare treated and non-treated samples (**$p < 0.02$). (D) Differentiated SH-SY5Y cells previously treated with 10 μM butyrolactone-I for 2 h, were incubated with 1% mannose, 45 mM NaCl, 45 mM KCl or 10 μM β-amyloid peptide. After 4 h, cells were harvested and subjected to Northern blot analysis using a [^{32}P]-labeled probe specific for human p19 mRNA and reprobed for β-tubulin mRNA. The figure is representative of three independent experiments with similar results. Densitometric analysis of p19 is represented in the right panel. Bars represent the mean ± S.D. of three experiments. Student's *t*-test was used to compare treated and non-treated samples (*$p < 0.05$; **$p < 0.02$). (E) Differentiated SH-SY5Y cells previously labeled with [^{32}P]-orthophosphate were treated as in D. After 2 h, equal amounts of whole cell extracts were used to analyze endogenous p19 phosphorylation by immunoprecipitation and autoradiography. The figure shows a representative autoradiograph of tree independent experiment with similar results. (F) Immunoprecipitated CDK5 from differentiated SH-SY5Y cells previously treated as in D was used to performed in vitro kinase assay. Measurements were done in triplicates and bars show the mean ± S.D. of three independent experiments. Student's *t*-test was used to compare treated and non-treated samples (*$p < 0.05$; **$p < 0.02$; ***$p < 0.01$, at least). (G) Differentiated SH-SY5Y cells were pre-incubated with 250 μM EGTA for 30 min and then treated with 10 μM β-amyloid peptide, 100 ng/ml neocarzinostatin or 45 mM KCl. After 4 h, the expression of p19 was analyzed by Northern blot. The figure is a representative of three independent experiments with similar results. Densitometric analysis of p19 is represented in the right panel. Bars represent the mean ± S.D. of three experiments. Student's *t*-test was used to compare treated and non-treated samples (*$p < 0.05$; **$p < 0.02$; ***$p < 0.01$). (H) Differentiated SH-SY5Y cells previously labeled with [^{32}P]-orthophosphate were treated as in G. After 2 h, the cells were harvested and equal amounts of whole protein extracts were used to analyze endogenous p19 phosphorylation by immunoprecipitation and autoradiography. The figure shows a representative autoradiograph of three independent experiments with similar results. (I) Differentiated SH-SY5Y cells previously labeled with [^{32}P]-orthophosphate were treated with 10 μM calpeptin for 2 h and then incubated with 10 μM β-amyloid peptide, 100 ng/ml neocarzinostatin or 5 μM A23187 for additional 2 h. Equal amounts of whole protein extracts were used to analyze endogenous p19 phosphorylation by immunoprecipitation and autoradiography. The figure shows a representative autoradiograph of three independent experiments with similar results. (J) In vitro CDK5 kinase assay was performed using immunoprecipitated CDK5 from differentiated SH-SY5Y cells previously treated as in I. Measurements were done in triplicates and bars show the mean ± S.D. of three independent experiments. Student's *t*-test was used to compare treated and non-treated samples (**$p < 0.02$; ***$p < 0.01$, at least). β-Amyloid peptide (β-am), mannose (Ma), butyrolactone-I (BL-I), neocarzinostatin (NCS), and optic densitometry (OD).

overexpressing calpain and co-transfected them with V5-tagged p19 wild type or mutant versions in which S76, the site of CDK5-mediated phosphorylation, was replaced by alanine or glutamic acid. In a previous work, we demonstrated that S76E mimics p19 phosphorylation [34]. As expected, p19wt-V5 levels were decreased in cells overexpressing calpain. Moreover, p19S76A-V5 levels were much lower in this condition. Conversely, expression levels of the p19S76ET141E-V5 mutant were not modified in cells transfected with a vector encoding calpain (Fig. 4F). As expected transfected calpain induced p35 cleavage partially inhibited by calpeptin treatment (Supplementary Fig. 4E). We measured CDK5 activity to confirm the activity of overexpressed calpain (Supplementary Fig. 4F). The results strongly suggest that S76-p19

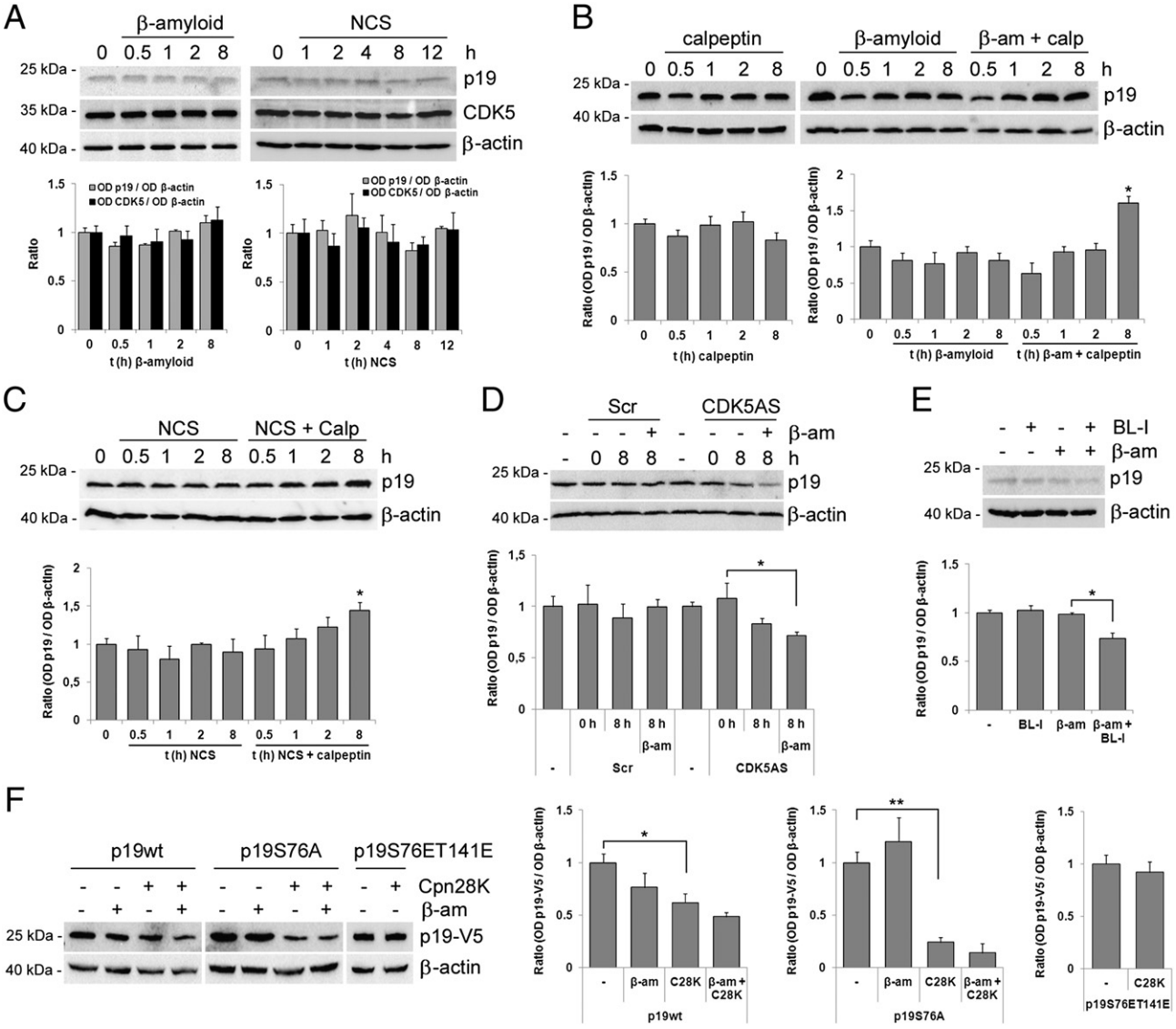

Fig. 4. CDK5-mediated phosphorylation stabilizes p19 protein. (A) Differentiated SH-SY5Y cells were incubated with 10 μM β-amyloid peptide or 100 ng/ml neocarzinostatin and cell lysates prepared at the indicated times. Western blot analysis of p19 and CDK5 were carried out with 20 μg of total cellular proteins and detected with p19 monoclonal antibody or CDK5 polyclonal antibody respectively. The figure is a representative of three independent experiments with similar results. Densitometric analysis of p19 and CDK5 is represented in the lower panels. Bars represent the mean ± S.D. of three experiments. (B and C) Differentiated SH-SY5Y cells were pre-treated with 10 μM calpeptin for 2 h and then incubated with 10 μM β-amyloid peptide (B) or 100 ng/ml neocarzinostatin (C). Cell lysates were prepared at the indicated times following DNA damage treatment and the expression of p19 protein was analyzed by Western blot. The figure is a representative of three (B) or four (C) independent experiments with similar results. Densitometric analyses of p19 are represented in the lower panels. Bars represent the mean ± S.D. of three or four experiments. Student's *t*-test was used to compare treated and non-treated samples (*$p < 0.05$). (D) Differentiated SH-SY5Y cells were transfected with an antisense oligodeoxynucleotide to CDK5 (CDK5AS) or its scrambled sequence (Scr). After 24 h, cells were treated with 10 μM β-amyloid peptide for an additional 8 h. Western blot analysis of p19 was carried out with 20 μg of total cellular proteins and detected with p19 monoclonal antibody. The figure is a representative of four independent experiments with similar results. Densitometric analysis of p19 is represented in the lower panel. Bars represent the mean ± S.D. of four experiments. Student's *t*-test was used to compare β-amyloid treated and CDK5AS transfected samples (*$p < 0.05$). (E) Differentiated SHSY5Y cells were pre-treated with 10 μM butyrolactone-I for 2 h and then incubated with 10 μM β-amyloid peptide. Cell lysates were prepared 8 h following damage treatment and the expression of p19 protein was analyzed by Western blot. Results are representative of three independent experiments with similar results. Densitometric analysis of p19 is represented in the lower panel. Bars represent the mean ± S.D. of three experiments. Student's *t*-test was used to compare treated and non-treated samples (*$p < 0.05$). (F) Differentiated SH-SY5Y cells were transiently co-transfected with expression vectors encoding the V5-tag in frame with wild type p19 (p19wt) or p19 mutants (p19S76A, p19S76ET141E) along with an expression vector encoding the 28 kDa small subunit of rat calpain (Cpn28K) and pBabe-Puro. Twenty-four hours after transfection, cells were treated with 1 μg/ml puromycin and incubated for another 24 h. Resistant SH-SY5Y cell were damaged with 10 μM β-amyloid peptide and collected 12 h after treatment. Western blot analysis of p19-V5 was carried out with 20 μg of total cellular proteins and detected with anti-V5 monoclonal antibody. The figure is a representative of three independent experiments with similar results. Densitometric analyses of p19 are represented in the right panels. Bars represent the mean ± S.D. of three experiments. Student's *t*-test was used to compare Cpn28K transfected and non-transfected samples (*$p < 0.05$; **$p < 0.02$). β-Amyloid peptide (β-am), neocarzinostatin (NCS), butyrolactone-I (BL-I), calpeptin (calp), Cpn28K (C28K), and optic densitometry (OD).

phosphorylation mediated by CDK5 plays a stabilizing role in p19 protein against calpain-mediated degradation.

3.5. p19 improves DNA repair, diminishes apoptosis and increases neuronal survival under genotoxic stress

As previously mentioned, p19 is a cell cycle inhibitor which has also a role in the DNA damage response. To determine whether p19 participates in the maintenance of DNA integrity in neuronal cells we first carried out an unscheduled DNA synthesis (UDS) assay in differentiated SH-SY5Y neuronal cells stably transfected with cDNA expressing p19 sense or p19 antisense driven by metallothionein promoter stimulated by Zn^{2+} addition to the culture medium. p19 expression was assessed by Northern blot and clones providing maximal and minimal p19 expression were selected (Supplementary Fig. 5A and B). In addition, expression of endogenous p19 was not affected by 100 μM Zn^{2+} (Supplementary Fig. 5C). We observed that β-amyloid-treated cells overexpressing the p19 sense displayed greater DNA repair synthesis than cells transfected with the empty vector (Fig. 5A). In contrast, DNA repair synthesis was markedly decreased in β-amyloid or NCS-treated cells overexpressing p19 antisense (Fig. 5A and Supplementary Fig. 5D). This decrease in UDS indicates not only that DNA repair enhancement results specifically from p19 overexpression but also that endogenous p19 is necessary to achieve a complete response to DNA damage. In addition, hippocampal neurons with deficient levels of p19 (Supplementary Fig. 5E) displayed a decreased DNA repair capacity after damage by β-amyloid peptide (Fig. 5B) or NCS (Supplementary Fig. 5F).

In view of the ability of p19 to maintain DNA integrity, we next attempted to find out whether apoptosis caused by DNA-damaging agents correlates with p19 levels. To do this, we determined the activity of caspase-3, an effector caspase that accomplishes the final cell death program, in differentiated SH-SY5Y cells expressing p19 sense or antisense deoxyoligonucleotide and rat hippocampal neurons with deficient levels of p19. The induction of caspase-3 activity revealed that neuronal cells underwent apoptosis after genotoxic damage (Fig. 5C and D). We also showed that Zn^{2+} addition to culture medium did not modify its activity (Supplementary Fig. 5G). The extent of induction of caspase-3 activity was decreased in cells transfected with the p19 sense deoxyoligonucleotide. Conversely, a significant increase in caspase-3 activity was observed in NCS-treated hippocampal neurons or SH-SY5Y cells with deficient levels of p19 (Fig. 5C and D). In addition, a similar increase was observed in β-amyloid-treated hippocampal neurons with deficient levels of p19 (Fig. 5D). Importantly, p19-deficient hippocampal neurons showed a significant greater level of caspase-3 activity even in the absence of genotoxics, suggesting that p19 displays a more general protective role in preserving genomic integrity (Fig. 5D).

To address whether the downregulation of p19 has any biological significance and plays any functional role in the cellular response upon genotoxic treatment, we examined cell survival in differentiated SH-SY5Y cells and neurons from rat hippocampus. Both p19-deficient neurons and SH-SY5Y cells overexpressing antisense p19 deoxyoligonucleotide were more sensitive to β-amyloid or NCS damage (Fig. 5E–G). On the other hand, we observed no significant differences in the cell survival of NCS-treated SH-SY5Y cells overexpressing sense p19 deoxyoligonucleotide (Supplementary Fig. 5H). Control assays showed that the presence of $ZnSO_4$ had no effect on cell proliferation (Supplementary Fig. 5I).

To further analyze the long-term effects and physiological relevance of p19 in cell survival in neurons, we performed clonogenic assays. The dose–response curve differed significantly depending on p19 status. We found that 99% and 73% of the colonies from p19 normal cells survived at 1 and 2 ng/ml NCS, respectively, while 62% and 41% remained alive at the same doses (Fig. 5H). Collectively, these results indicate that p19 influences neuronal sensitivity to DNA damagers thus providing a remarkable advantage against genotoxic stress.

3.6. In vivo p19 deficiency makes hippocampal cells more sensitive to genotoxic stress

Next, we examined whether the neuroprotective properties of p19 could be recapitulated in an in vivo mouse model. To do this, a single-stranded DNA oligonucleotide containing an antisense sequence of p19 was laterally injected by stereotaxis in the dorsal hippocampus to selectively knock down the p19 expression (Fig. 6A). The injected oligodeoxynucleotide was able to decrease p19 expression in the hippocampus and Neu-2a cells (Supplementary Fig. 6A and B). A scrambled oligodeoxynucleotide, injected in the contralateral hippocampus was used as a control for the non-specific actions of DNA administration. After 16 h, 0.5 ml of 25 ng/ml NCS or saline solution was administered in each hippocampus. The time and concentration to which genotoxic was injected arose from a time- and dose–response curves performed previously (Supplementary Fig. 6C). The NCS concentration selected represents the minimum dose of genotoxic that causes a significant DNA damage measured as the number of γH2AX-positive cells. Brain sections were examined 24 h later for γH2AX immunoreactivity to label DNA damaged cells. Administration of NCS in the dorsal region of the hippocampus caused an increase in γH2AX-positive cells. Importantly, the number of DNA damaged cells was almost two-fold higher in the hippocampus from mice previously injected with p19 antisense oligodeoxynucleotide (Fig. 6B and C). Interestingly, in the absence of genotoxic administration, a slight but significant increase in γH2AX-positive cells was observed in the hippocampus from mice injected with the p19 antisense deoxyoligonucleotide compared with those injected with the scrambled one. These results strongly support a role of p19 in the maintenance of genomic integrity in the mouse hippocampus.

3.7. Mice with a p19 hippocampal deficiency display impairment of cognitive skills after genotoxic stress

In view of the fact that the presence of p19 contributes to attenuating the effect of genotoxics to DNA integrity in the hippocampus of the mouse brain, we hypothesize that p19 could ameliorate the adverse consequences on hippocampus-dependent tasks in a brain exposed to DNA stressors. To test this hypothesis, mouse brains were bilaterally injected in the dorsal hippocampus with p19 antisense (ASp19) or scrambled (Scr) oligodeoxynucleotides. Sixteen hours later, mice were injected with either NCS or saline solution. Hippocampal-dependent learning and memory of mice were studied using Y-maze tests. Working memory was first assessed using the spontaneous alternation procedure, a non-aversive task based on exploratory behavior and allowing differentiation between mnesic and locomotor behaviors. One-way ANOVA indicated that spontaneous alternation behavior in the Y-maze was affected by the treatment ($F_{2,29} = 11.52$, $p = 0.0002$). Bonferroni post hoc comparisons showed a significant decrease in the spontaneous alternation in ASp19 + NCS treated-mice compared with Scr + saline ($t_{18} = 4.697$, $p < 0.001$) or with Scr + NCS ($t_{18} = 3.207$, $p < 0.05$) (Fig. 7A). This observation could not be attributed to an effect on the motor activity because the total distance traveled (Fig. 7B) and the number of arm entries (Fig. 7C) in the Y-maze task was not significantly different between the groups. This observation can neither be attributed to an aversive behavior because the distance traveled (Supplementary Fig. 7A–C) and the time spent (Supplementary Fig. 7D–F) in each arm was not different between the three groups. These results suggest a deleterious effect of the deficient expression level of p19 on short-term spatial memory.

Next, mice from all three groups were evaluated in spatial learning using a two-trial recognition memory test with the Y-maze device. Mice from the Scr + saline and Scr + NCS groups entered more

frequently and spent more time in the novel previously unvisited arm of the maze. No significant differences were observed between both groups (arm entry: $t_{18} = 0.7610$, $p = 0.2283$; dwell time: $t_{18} = 0.3613$, $p = 0.3610$) (Supplementary Fig. 8A and B). In contrast, the ASp19 + NCS group mice showed no preference toward the novel arm and entered the different arms randomly (arm entry: $t_{18} = 1.812$, $p = 0.0434$; dwell time: $t_{18} = 2.665$, $p = 0.0079$). The deficit in spatial memory of ASp19 + NCS mice was evident also when the arm chosen for the first entry was compared with that chosen by Scr + saline mice group ($\chi^2 = 3.810$, $df = 1$, $p = 0.0255$) (Fig. 7D). Conversely, most Scr + saline and Scr + NCS mice groups selected the novel arm as the first choice, and no significant differences were observed between both groups ($\chi^2 = 0.3922$, $df = 1$, $p = 0.2656$).

We next performed a fear conditioning test to further evaluate the consequences of p19 deficiency in the hippocampus in a DNA damage context. Mice were trained using the Pavlovian fear conditioning paradigm 24 h before a memory test. One-way ANOVA indicated that the freezing behavior of mice was affected by the treatment ($F_{2,25} = 6.255$, $p = 0.0063$) (Fig. 7E). Bonferroni post hoc analysis revealed that ASp19 + NCS mice exhibited significantly reduced freezing behavior than Scr + saline ($t_{16} = 2.780$, $p < 0.05$) and than Scr + NCS mice ($t_{17} = 3.304$, $p < 0.01$). Consistent with the notion that the hippocampus is not required for cued fear conditioning [43], the two-way ANOVA showed no significant differences for treatment ($F_{2,27} = 0.4668$, $p = 0.8831$) in the tone-dependent memory test (Fig. 7F). Next, mice were subjected to a novel object recognition task that relies

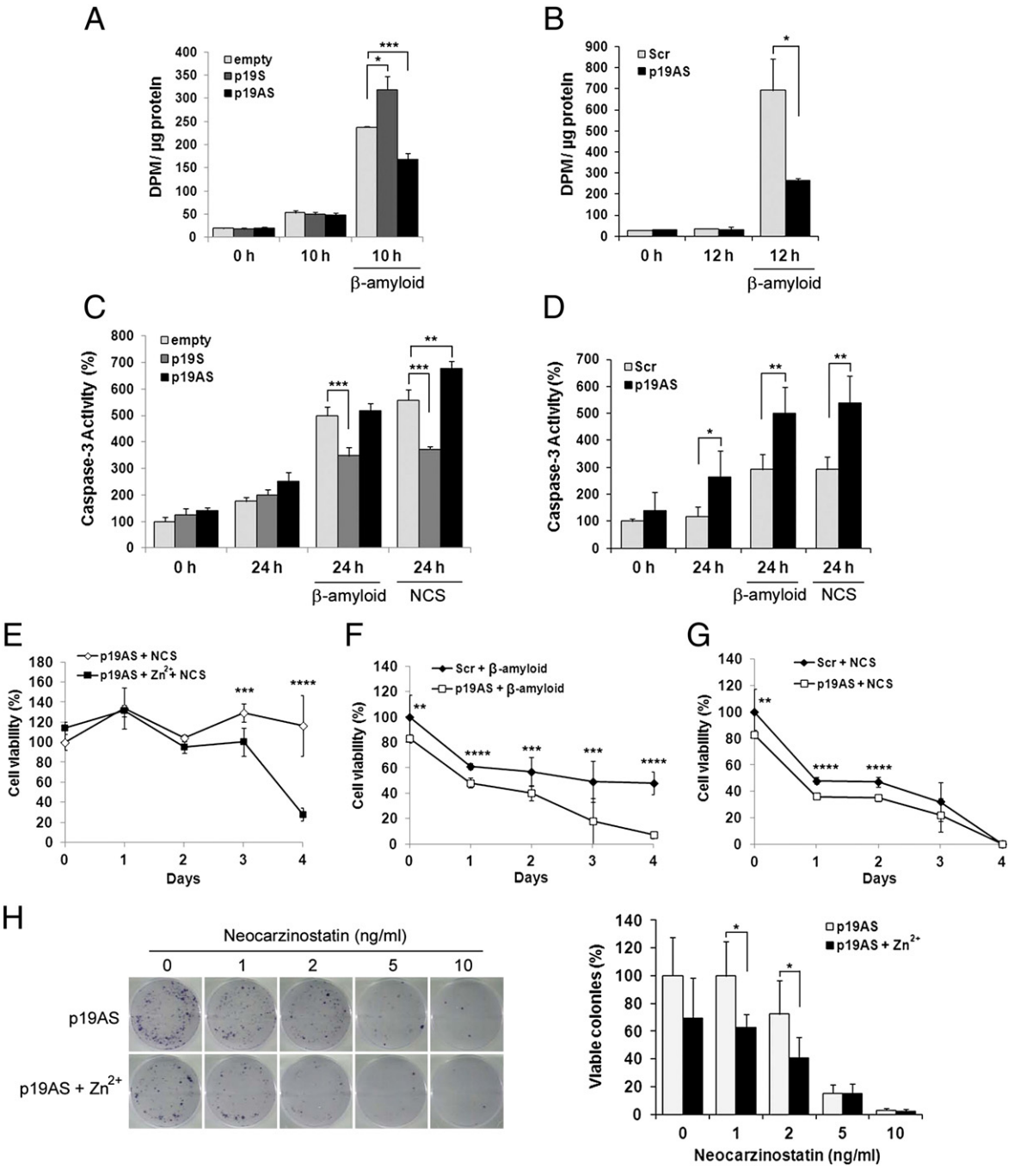

on the mouse's natural exploratory behavior. No differences in the time spent exploring the novel object were observed between the three groups ($F_{2,26} = 0.4180$, $p = 0.6627$) (Supplementary Fig. 8C).

Finally, mouse performance in non-hippocampus-dependent tasks was similar in all the three groups tested. Neither the neuromuscular coordination, evaluated by means of tightrope test, nor the muscle strength, assessed in a hangwire test, showed significant differences between groups (Supplementary Fig. 8D and E). Likewise, no forelimb asymmetries, assessed in the rearing test, were detected in mice of any of the three groups (Supplementary Fig. 8 F).

4. Discussion

Neurons formed during early development are preserved for life and therefore face the task of maintaining a stable genome for long periods of time. DNA damage, which perturbs genomic stability, has been related to cognitive decline in the aging human brain [44]. In addition, mutations in DNA-repair genes have neurological implications [45]. Several studies have suggested that DNA damage is also increased in disorders such as Alzheimer's disease, Parkinson's disease and amyotrophic lateral sclerosis [7,46]. However, the precise mechanisms connecting DNA damage with neurodegeneration remain poorly understood.

Overall, our data show that p19 contributes to the maintenance of genomic integrity in nervous system cells challenged by neurotoxic conditions preserving their functionality. We found that exposure of differentiated human neuroblastoma cells or rat hippocampal neurons to β-amyloid peptide or NCS induce changes in p19 cellular status including transcriptional activation and protein phosphorylation. p19 induction and phosphorylation are also accomplished by the increase in intracellular calcium. Increased intracellular calcium levels trigger the depolarization of mitochondrial membrane and subsequent loss of membrane potential, which is accompanied by the generation of ROS which, in turn, cause DNA damage [47].

It has been previously demonstrated that p19 protein contains a CDK phosphorylation site located in Ser 76 that is crucial for p19 function in DNA repair and cell survival [34]. The data presented in this study indicate that CDK5 is specifically involved in p19 phosphorylation in response to DNA damage. Several results support this statement. First, differentiated SH-SY5Y cells incubated with CDK5 antisense deoxyoligonucleotide, but not with CDK2 antisense, resulted in the inhibition of DNA damage-mediated p19 phosphorylation. Second, cells treated with butyrolactone-I, a CDK5 inhibitor, abolished p19 phosphorylation. Finally, reconstituted CDK5 activity in non-neuronal cells not expressing endogenous CDK5 activity recapitulates p19 phosphorylation in the absence of DNA damage stimuli. Together, these findings indicate that CDK5 activation and p19 phosphorylation in postmitotic neurons may represent a mode of response to a wider spectrum of signals.

The protease calpain is known to be stimulated under genotoxic stress, increased intracellular calcium or neurological damage conditions [48,49]. In these conditions, CDK5 hyperactivation results from the accumulation of p25 from the cleavage of p35 by pathogenic activation of calpain. p25 is more stable than p35 and thereby maintains CDK5 in a hyperactive state. The binding of p25 to CDK5 is also thought to change CDK5 subcellular localization from the plasma membrane to the cytoplasm and nucleus, potentially altering CDK5 substrate specificity [50]. Although the identity and localization of these pathogenic substrates were first unclear, recent reports have shown that aberrant cytoplasm CDK5 activity phosphorylates peroxiredoxin-2, decreasing its peroxidase activity and decreasing the capacity of cells to reduce ROS [51]. Furthermore, the apurinic/apyrimidinic endonuclease 1, which plays an essential role in the base excision repair pathway, has been recently identified as a target of the nuclear CDK5 activity, interfering with the repair of this type of DNA damage [52]. This dysregulation of CDK5, found in neuronal DNA damage response, is neurotoxic and may contribute to the pathogenesis of neurodegenerative disorders.

In this regard, the inhibition of calpain with the inhibitor calpeptin clearly decreased not only CDK5 activity, but also p19 phosphorylation. This close correlation suggests an upstream pathway for p19 phosphorylation formed by calpain activation, p35 to p25 cleavage and subsequent increased CDK5 activity. Since p19 is also targeted by calpain-protease activity CDK5-mediated p19 phosphorylation was crucial to increase its stability. The fact that p19S76A mutant levels were rapidly decreased in response to genotoxics while its counterpart in which Ser76 was changed by a negative charged aminoacid mimic the phosphate residue did not, correlate in support.

Besides its phosphorylation, we demonstrated that in response to DNA damage p19 expression is transcriptionally induced and mediated by E2F transcription factors. These findings prompted us to hypothesize that the p19 protein level observed in neuronal cells treated with β-amyloid peptide or NCS is the result of a dynamic equilibrium

Fig. 5. p19 enhances the ability to repair DNA lesions and confers resistance to β-amyloid and neocarzinostatin in neuronal cells. (A) Differentiated SH-SY5Yempty, SH-SH5Yp19S or SH-SY5Yp19AS cells were maintained in a medium containing 0.5% fetal bovine serum during 24 h, and incubated with 100 μM $ZnSO_4$ for another 16 h. After this time, cells were treated with 10 μM β-amyloid peptide, incubated with 10 μCi [^{3}H]thymidine and cell lysates were tested for UDS assay at different time points. Bars represent the mean ± S.D. of three different experiments performed in triplicate. Student's t-test was used to compare β-amyloid-treated p19 sense or antisense stable transfectant samples with β-amyloid-treated empty vector stable transfectant samples at 10 h (*$p < 0.05$; ***$p < 0.01$). (B) Hippocampal neurons were transfected with p19 antisense oligonucleotide (p19AS) or its scrambled sequence (Scr) and, 24 h later, incubated with 10 μM β-amyloid peptide and 10 μCi/ml [^{3}H]-thymidine. Following 12 h, cell lysates were tested for UDS assay. Bars represent the mean ± S.D. of three different experiments performed in triplicate. Student's t-test was used to compare β-amyloid-treated p19AS transfectant samples with β-amyloid-treated Scr transfectant samples at 12 h (*$p < 0.05$). (C) Differentiated SH-SY5Yp19S, SH-SY5Yp19AS or SH-SY5Yempty cells were maintained in a medium containing 100 μM $ZnSO_4$ during 16 h. After this time, cells were treated with 10 μM β-amyloid peptide or 100 ng/ml neocarzinostatin. Twenty-four hours later, cell lysates were tested for caspase-3 activity. Results are expressed as percentage of caspase-3 activity with respect to basal activity of cell lysates stably transfected with empty vector and without damage treatment, which was set to 100. Bars represent the mean ± S.D. of three independent experiments performed in quadruplicate. Student's *t*-test was used to compare β-amyloid-treated or NCS-treated p19 sense or antisense stable transfectants samples with β-amyloid-treated or NCS-treated empty vector stable transfectant samples at 24 h (**$p < 0.02$; ***$p < 0.01$, at least). (D) Hippocampal neurons were transfected with p19 antisense oligonucleotide (p19AS) or its scrambled sequence (Scr) and, 24 h later, incubated with 10 μM β-amyloid peptide or 50 ng/ml neocarzinostatin. Immediately and 24 h after damage, cell lysates were tested for caspase-3 activity. Results are expressed as percentage of caspase-3 activity with respect to basal activity of cell lysates transfected with scrambled oligonucleotide and without damage treatment measured at time point 0 h, which was set to 100. Bars represent the mean ± S.D. of three independent experiments performed in quadruplicate. Student's t-test was used to compare p19AS transfectant samples with Scr transfectant samples at time point 24 h (*$p < 0.05$; **$p < 0.02$). (E) Differentiated SH-SY5Yp19AS were maintained in basal medium or medium containing 100 μM $ZnSO_4$ during 16 h. After this time, cells were treated with 50 ng/ml neocarzinostatin. At the indicated times, cell viability was assessed by MMT reduction assay. Results are expressed at percentage of cell viability with respect to viability of p19AS cells without $ZnSO_4$ treatment measured at time point 0 day, which was set to 100. Bars represent the mean ± S.D. of three independent experiments performed in sextuplicate. Student's t-test was used to compare $ZnSO_4$ treated samples and $ZnSO_4$ non-treated samples (***$p < 0.01$; ****$p < 0.005$). (F and G) Hippocampal neurons were transfected with p19 antisense oligonucleotide (p19AS) or its scrambled sequence (Scr) and, 24 h later, incubated with 10 μM β-amyloid peptide (F) or 50 ng/ml neocarzinostatin (G). At the indicated times, cell viability was assessed by MMT reduction assay. Results are expressed at percentage of cell viability with respect to viability of cells transfected with scrambled oligonucleotide measured at time point zero day, which was set to 100. Bars represent the mean ± S.D. of three independent experiments performed in sextuplicate. Student's t-test was used to compare p19AS transfected samples and scrambled transfected samples (**$p < 0.02$; ***$p < 0.01$; ****$p < 0.005$). (H) Clonogenic survival was assessed in SH-SY5Yp19AS clonal cell line during 10 days after neocarzinostatin treatment. Left panel shows representative colony images of each treatment. Right panel shows the quantification of viable colonies. Results are expressed at percentage of viable colonies with respect to colonies of untreated cells, which was set to 100. Bars represent the mean ± S.D. of three independent experiments performed in sextuplicate. Student's t-test was used to compare $ZnSO_4$ treated samples and $ZnSO_4$ non-treated samples (*$p < 0.05$). Neocarzinostatin (NCS).

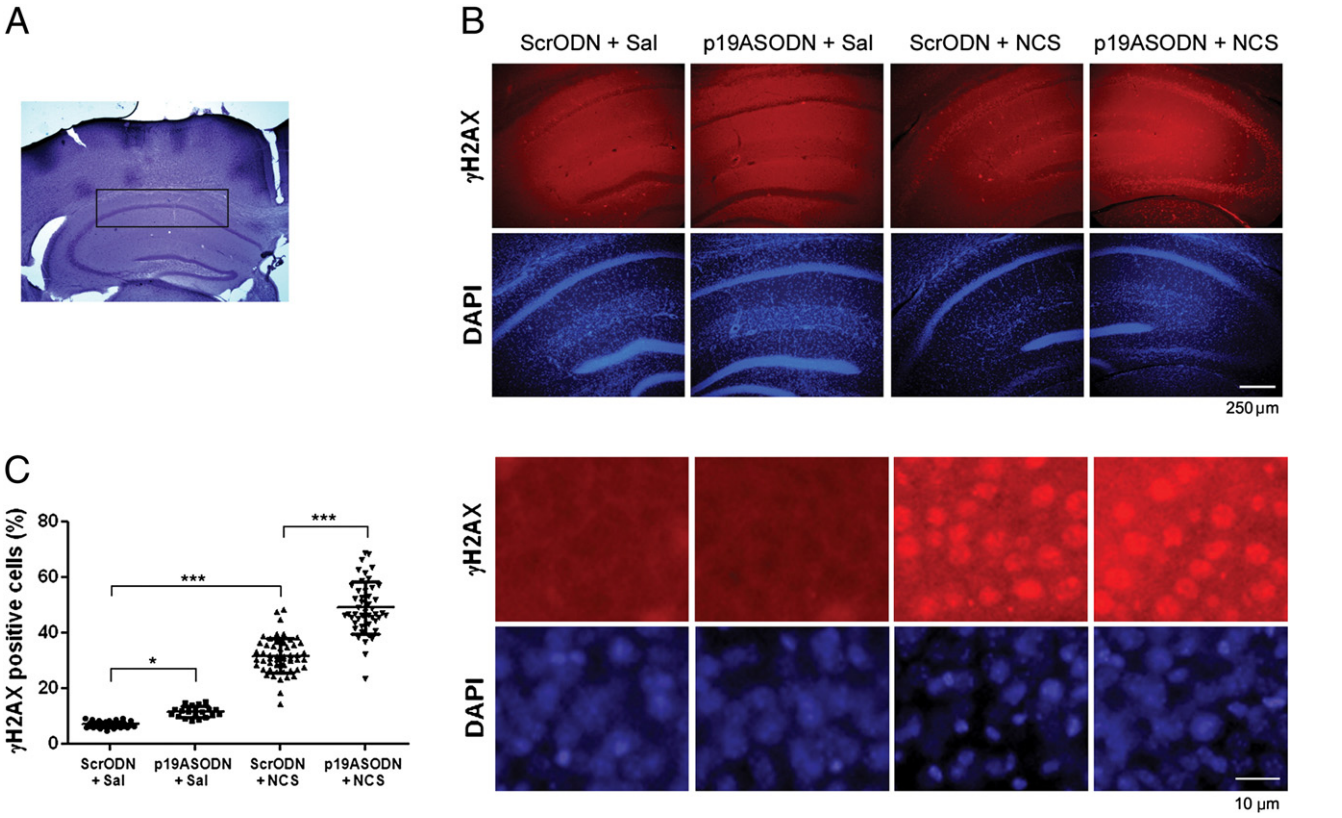

Fig. 6. p19 deficiency make hippocampal cells more sensitive to genotoxic stress. (A) The figure shows a representative image of the area affected by ODNs and NCS (40× magnification). (B) Cannulated mice were injected with p19ASODN in the dorsal hippocampus and with ScrODN in the contra lateral dorsal hippocampus. Sixteen hours later, mice were injected with 25 ng/ml NCS or vehicle (saline) in both hippocampi. The presence of γH2AX was analyzed in coronal sections 24 h after injections by immunofluorescence. Nuclei were stained with DAPI (100× magnification — scale bar: 250 μm, upper panels; 400× magnification — scale bar: 10 μm, lower panels). (C) Scatter plot showing the percentage of γH2AX-positive cells in hippocampus slices of ScrODN + Sal (n = 41 slices), p19ASODN + Sal (n = 21 slices), ScrODN + NCS (n = 57 slices), and p19ASODN + NCS (48 slices) mice. One way ANOVA indicates significant differences by the treatment ($F_{3,163} = 386.5$, $p < 0.0001$). Bonferroni post hoc comparisons show significant differences between treatments ($^{*}p < 0.05$, $^{***}p < 0.001$). Scrambled (Scr), oligodeoxynucleotide (ODN), saline (Sal), and neocarzinostatin (NCS).

between the increased synthesis caused by the E2F-mediated transcriptional induction and the increased degradation produced by the activation of calpain.

Aberrant cell cycle activity and DNA damage are emerging as important pathological components in various neurodegenerative conditions. Unlike proliferating cells, in which DNA damage typically triggers cell-cycle checkpoints, postmitotic neurons activate their cell cycle machinery, under stress conditions, including genotoxic stimulation [53]. This cell cycle re-entry by postmitotic neurons leads to neuronal death; inhibition of such ectopic cell cycle activity protects neurons [54]. Previous work demonstrated that the CDK inhibitors p19 and p27Kip1 are rate limiting for neuronal terminal differentiation and suggested that they are integral components of the molecular machinery that keeps postmitotic neurons from re-entering the cell cycle after they migrate to their final position [55]. Here, we showed that during the differentiation process triggered by ATRA in human neuroblastoma cells, p19 expression was increased in an Egr-1 dependent manner. Egr-1, an immediate early gene, is a Zn-finger transcription factor identified as a key molecule in the regulation of cell division, differentiation and apoptosis [56]. It has been reported that Egr-1 displays a functional role in the process of neuronal death promoted by DNA damage [22]. Egr-1 would induce p35 expression leading to the subsequent CDK5 activation by a mechanism other than calpain-mediated p35-cleavage. Considering these, and our present results, the high level of p19 in differentiated neurons would have two related consequences: the maintenance of the postmitotic state and the protection of neurons from neurotoxic stimuli.

The results obtained in the cultures of neuronal cells and in the in vivo experiments underscore the physiological relevance of p19 in the maintenance of genomic integrity. p19 expression increased the cellular ability to repair damaged DNA and decreased the genotoxic-induced apoptosis in neuronal cells. Most importantly, p19 deficiency sensitized hippocampal cells to the genotoxic activity of NCS. The genomic integrity protection provided by p19 seems to have a functional relevance. Hippocampus-dependent learning and memory tasks were better preserved from genotoxic damage when p19 expression was allowed in this brain region.

Based on all the above, we propose a feedback mechanism by which the neurotoxic effects of CDK5-p25 activated by genotoxic stress or abnormal intracellular calcium levels are counteracted by the induction and stabilization of p19 protein reducing the adverse consequences on the brain functions. Thus, both beneficial and adverse signals can be triggered by the deregulation of CDK5/p25 activity. The protective effect exerted by p19 would not only be linked to a genotoxic acute damage. In neurodegenerative disorders such as Alzheimer's disease, Parkinson's disease and amyotrophic lateral sclerosis, the main risk factor is age itself [57]. Analysis of postmortem human brain samples has shown an association between the downregulation of genes encoding for learning and memory with increased amounts of oxidative damage in the promoters of the downregulated genes [44]. DNA damage induced by ROS has the potential to block transcription by RNA polymerase II, and their accumulation in repair-defective individuals may cause neuronal cell death, either by progressively depriving the cell of vital transcripts or through apoptosis [58]. These evidences raise the possibility that the accumulation of DNA damage with age could underlie the pathological changes that are related to neurological disease. In this scenario, the action of proteins allowing a more robust response against DNA damage and, in consequence, avoiding excessive apoptosis or

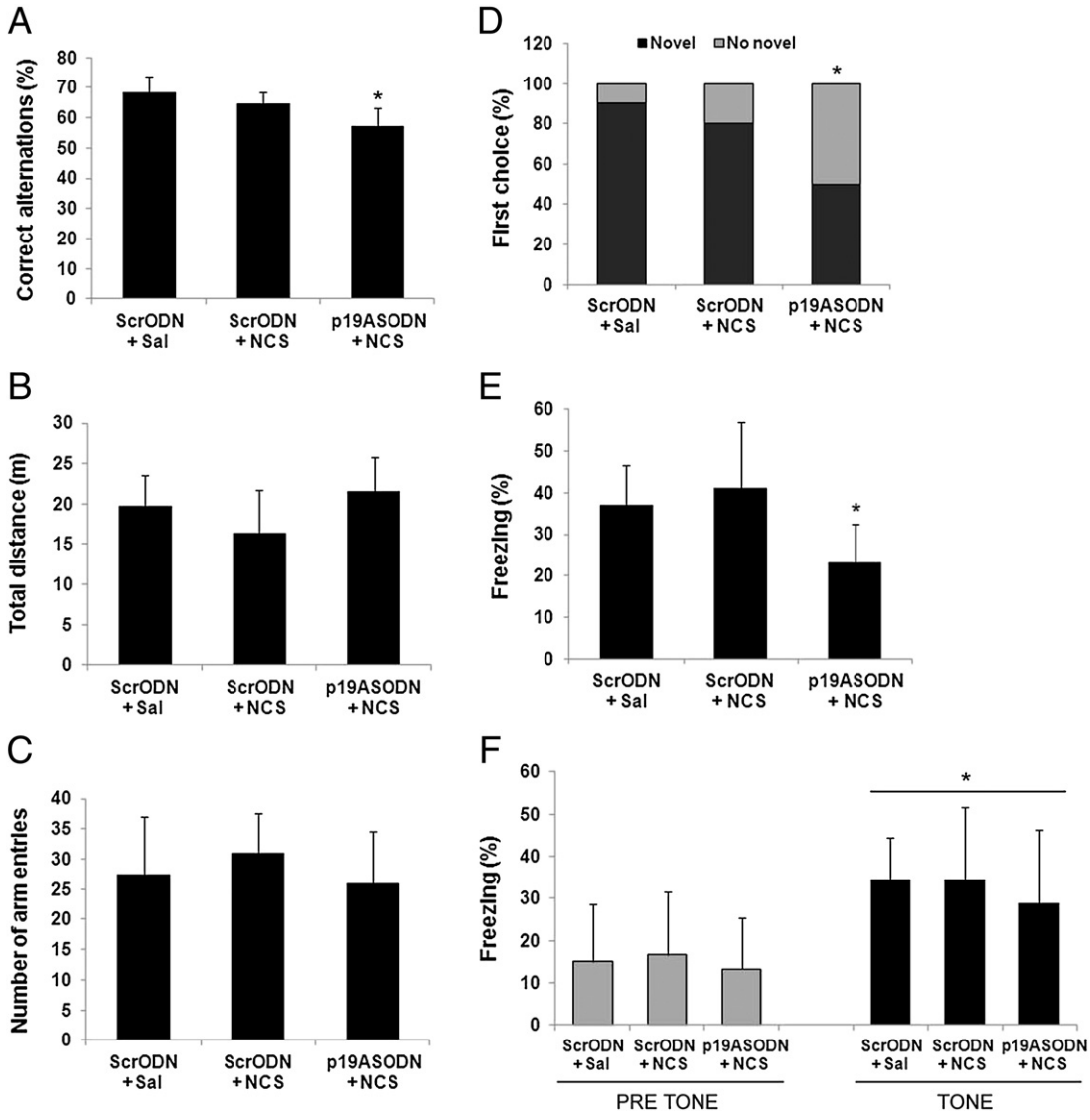

Fig. 7. Impaired hippocampal learning and memory in DNA-damaged p19-deficient mice. Cannulated mice were bilaterally injected with 0.5 μl of 1 ng/ml p19ASODN or ScrODN in the dorsal hippocampus. Sixteen hours later, mice were injected with 25 ng/ml NCS or vehicle (saline) in both hippocampi. After one week, mice from the three groups were subjected to the following cognitive tests. (A, B and C) Mice Performance in Y-maze device, showing percentage of (A) correct spontaneous alternations, (B) total distance traveled and (C) total number of arm entries. (D) Percentage of animals selecting the novel arm as the first choice in cued Y-maze. (E) Contextual memory evaluated by the fear conditioning test. The figure compares mean values of freezing of the three groups. (F) Mice were tested to the cued fear conditioning, one day after the contextual test. Freezing response was measured during pre-tone and tone periods. ScrODN + Sal ($n = 10$), ScrODN + NCS ($n = 10$) and p19ASODN + NCS ($n = 10$). In all cases bars represent the mean ± S.D.

senescence is highly advantageous. The reported ability of p19 in maintaining genomic integrity would adjust to this premise. Considering these observations the benefits provided by p19 activation could be substantial.

Appendix A. Supplementary data

Supplementary data to this article can be found online at http://dx.doi.org/10.1016/j.bbamcr.2014.03.026.

References

[1] E.B. Becker, A. Bonni, Cell cycle regulation of neuronal apoptosis in development and disease, Prog. Neurobiol. 72 (2004) 1–25.
[2] A. Barzilai, DNA damage, neuronal and glial cell death and neurodegeneration, Apoptosis 15 (2010) 1371–1381.
[3] M.P. Dekkers, Y.A. Barde, Developmental biology. Programmed cell death in neuronal development, Science 340 (2013) 39–41.
[4] R.R. Buss, W. Sun, R.W. Oppenheim, Adaptive roles of programmed cell death during nervous system development, Annu. Rev. Neurosci. 29 (2006) 1–35.
[5] D.G. Southwell, M.F. Paredes, R.P. Galvao, D.L. Jones, R.C. Froemke, J.Y. Sebe, C. Alfaro-Cervello, Y. Tang, J.M. Garcia-Verdugo, J.L. Rubenstein, S.C. Baraban, A. Alvarez-Buylla, Intrinsically determined cell death of developing cortical interneurons, Nature 491 (2012) 109–113.
[6] M. Suzanne, H. Steller, Shaping organisms with apoptosis, Cell Death Differ. 20 (2013) 669–675.
[7] Y. Shen, P. He, Z. Zhong, C. McAllister, K. Lindholm, Distinct destructive signal pathways of neuronal death in Alzheimer's disease, Trends Mol. Med. 12 (2006) 574–579.
[8] M. Vila, S. Przedborski, Targeting programmed cell death in neurodegenerative diseases, Nat. Rev. Neurosci. 4 (2003) 365–375.
[9] A. Barzilai, S. Biton, Y. Shiloh, The role of the DNA damage response in neuronal development, organization and maintenance, DNA Repair (Amst) 7 (2008) 1010–1027.
[10] J.A. Klein, S.L. Ackerman, Oxidative stress, cell cycle, and neurodegeneration, J. Clin. Invest. 111 (2003) 785–793.
[11] P.J. McKinnon, DNA repair deficiency and neurological disease, Nat. Rev. Neurosci. 10 (2009) 100–112.
[12] A. Bender, K.J. Krishnan, C.M. Morris, G.A. Taylor, A.K. Reeve, R.H. Perry, E. Jaros, J.S. Hersheson, J. Betts, T. Klopstock, R.W. Taylor, D.M. Turnbull, High levels of mitochondrial DNA deletions in substantia nigra neurons in aging and Parkinson disease, Nat. Genet. 38 (2006) 515–517.
[13] P. Mao, P.H. Reddy, Aging and amyloid beta-induced oxidative DNA damage and mitochondrial dysfunction in Alzheimer's disease: implications for early intervention and therapeutics, Biochim. Biophys. Acta 1812 (2011) 1359–1370.

[14] F. Rodier, J.P. Coppe, C.K. Patil, W.A. Hoeijmakers, D.P. Munoz, S.R. Raza, A. Freund, E. Campeau, A.R. Davalos, J. Campisi, Persistent DNA damage signalling triggers senescence-associated inflammatory cytokine secretion, Nat. Cell Biol. 11 (2009) 973–979.
[15] G. Sulli, R. Di Micco, F. d'Adda di Fagagna, Crosstalk between chromatin state and DNA damage response in cellular senescence and cancer, Nat. Rev. Cancer 12 (2012) 709–720.
[16] R. Dhavan, L.H. Tsai, A decade of CDK5, Nat. Rev. Mol. Cell Biol. 2 (2001) 749–759.
[17] S. Jessberger, F.H. Gage, A.J. Eisch, D.C. Lagace, Making a neuron: Cdk5 in embryonic and adult neurogenesis, Trends Neurosci. 32 (2009) 575–582.
[18] F. Sananbenesi, A. Fischer, X. Wang, C. Schrick, R. Neve, J. Radulovic, L.H. Tsai, A hippocampal Cdk5 pathway regulates extinction of contextual fear, Nat. Neurosci. 10 (2007) 1012–1019.
[19] J.C. Cruz, L.H. Tsai, A Jekyll and Hyde kinase: roles for Cdk5 in brain development and disease, Curr. Opin. Neurobiol. 14 (2004) 390–394.
[20] F. Raynaud, A. Marcilhac, Implication of calpain in neuronal apoptosis. A possible regulation of Alzheimer's disease, FEBS J. 273 (2006) 3437–3443.
[21] M.J. O'Hare, N. Kushwaha, Y. Zhang, H. Aleyasin, S.M. Callaghan, R.S. Slack, P.R. Albert, I. Vincent, D.S. Park, Differential roles of nuclear and cytoplasmic cyclin-dependent kinase 5 in apoptotic and excitotoxic neuronal death, J. Neurosci. 25 (2005) 8954–8966.
[22] J.H. Lee, K.T. Kim, Regulation of cyclin-dependent kinase 5 and p53 by ERK1/2 pathway in the DNA damage-induced neuronal death, J. Cell. Physiol. 210 (2007) 784–797.
[23] M.A. Al-Mohanna, H.H. Al-Khalaf, N. Al-Yousef, A. Aboussekhra, The p16INK4a tumor suppressor controls p21WAF1 induction in response to ultraviolet light, Nucleic Acids Res. 35 (2007) 223–233.
[24] J.M. Ceruti, M.E. Scassa, J.M. Flo, C.L. Varone, E.T. Canepa, Induction of p19INK4d in response to ultraviolet light improves DNA repair and confers resistance to apoptosis in neuroblastoma cells, Oncogene 24 (2005) 4065–4080.
[25] J.M. Ceruti, M.E. Scassa, M.C. Marazita, A.C. Carcagno, P.F. Sirkin, E.T. Canepa, Transcriptional upregulation of p19INK4d upon diverse genotoxic stress is critical for optimal DNA damage response, Int. J. Biochem. Cell Biol. 41 (2009) 1344–1353.
[26] M.E. Scassa, M.C. Marazita, J.M. Ceruti, A.L. Carcagno, P.F. Sirkin, M. Gonzalez-Cid, O. P. Pignataro, E.T. Canepa, Cell cycle inhibitor, p19INK4d, promotes cell survival and decreases chromosomal aberrations after genotoxic insult due to enhanced DNA repair, DNA Repair (Amst) 6 (2007) 626–638.
[27] L. Tavera-Mendoza, T.T. Wang, B. Lallemant, R. Zhang, Y. Nagai, V. Bourdeau, M. Ramirez-Calderon, J. Desbarats, S. Mader, J.H. White, Convergence of vitamin D and retinoic acid signalling at a common hormone response element, EMBO Rep. 7 (2006) 180–185.
[28] E.T. Canepa, M.E. Scassa, J.M. Ceruti, M.C. Marazita, A.L. Carcagno, P.F. Sirkin, M.F. Ogara, INK4 proteins, a family of mammalian CDK inhibitors with novel biological functions, IUBMB Life 59 (2007) 419–426.
[29] J.J. Cunningham, M.F. Roussel, Cyclin-dependent kinase inhibitors in the development of the central nervous system, Cell Growth Differ. 12 (2001) 387–396.
[30] F. Zindy, H. Soares, K.H. Herzog, J. Morgan, C.J. Sherr, M.F. Roussel, Expression of INK4 inhibitors of cyclin D-dependent kinases during mouse brain development, Cell Growth Differ. 8 (1997) 1139–1150.
[31] S.B. Rosso, D. Sussman, A. Wynshaw-Boris, P.C. Salinas, Wnt signaling through Dishevelled, Rac and JNK regulates dendritic development, Nat. Neurosci. 8 (2005) 34–42.
[32] M.F. Ogara, P.F. Sirkin, A.L. Carcagno, M.C. Marazita, S.V. Sonzogni, J.M. Ceruti, E.T. Canepa, Chromatin relaxation-mediated induction of p19INK4d increases the ability of cells to repair damaged DNA, PLoS ONE 8 (2013) (2013) e61143.
[33] J.M. Ceruti, M.F. Ogara, C. Menendez, I. Palmero, E.T. Canepa, Inhibitor of growth 1 (ING1) acts at early steps of multiple DNA repair pathways, Mol. Cell. Biochem. 378 (2013) 117–126.
[34] M.C. Marazita, M.F. Ogara, S.V. Sonzogni, M. Marti, N.J. Dusetti, O.P. Pignataro, E.T. Canepa, CDK2 and PKA mediated-sequential phosphorylation is critical for p19INK4d function in the DNA damage response, PLoS ONE 7 (2012) (2012) e35638.
[35] K.B.J. Franklin, G. Paxinos, The Mouse Brain in Stereotaxic Coordinates, Academic Press, London, 2007.
[36] D.Y. Chen, S.A. Stern, A. Garcia-Osta, B. Saunier-Rebori, G. Pollonini, D. Bambah-Mukku, R.D. Blitzer, C.M. Alberini, A critical role for IGF-II in memory consolidation and enhancement, Nature 469 (2011) 491–497.
[37] Z. Sarnyai, E.L. Sibille, C. Pavlides, R.J. Fenster, B.S. McEwen, M. Toth, Impaired hippocampal-dependent learning and functional abnormalities in the hippocampus in mice lacking serotonin(1A) receptors, Proc. Natl. Acad. Sci. U. S. A. 97 (2000) 14731–14736.
[38] V. de la Fuente, R. Freudenthal, A. Romano, Reconsolidation or extinction: transcription factor switch in the determination of memory course after retrieval, J. Neurosci. 31 (2011) 5562–5573.
[39] A. Alvarez, J.P. Munoz, R.B. Maccioni, A Cdk5-p35 stable complex is involved in the beta-amyloid-induced deregulation of Cdk5 activity in hippocampal neurons, Exp. Cell Res. 264 (2001) 266–274.
[40] D. Kim, C.L. Frank, M.M. Dobbin, R.K. Tsunemoto, W. Tu, P.L. Peng, J.S. Guan, B.H. Lee, L.Y. Moy, P. Giusti, N. Broodie, R. Mazitschek, I. Delalle, S.J. Haggarty, R.L. Neve, Y. Lu, L.H. Tsai, Deregulation of HDAC1 by p25/Cdk5 in neurotoxicity, Neuron 60 (2008) 803–817.
[41] J. Qu, T. Nakamura, G. Cao, E.A. Holland, S.R. McKercher, S.A. Lipton, S-nitrosylation activates Cdk5 and contributes to synaptic spine loss induced by beta-amyloid peptide, Proc. Natl. Acad. Sci. U. S. A. 108 (2011) 14330–14335.
[42] J. Joy, N. Nalabothula, M. Ghosh, O. Popp, M. Jochum, W. Machleidt, S. Gil-Parrado, T. A. Holak, Identification of calpain cleavage sites in the G1 cyclin-dependent kinase inhibitor p19(INK4d), Biol. Chem. 387 (2006) 329–335.
[43] R.G. Phillips, J.E. LeDoux, Differential contribution of amygdala and hippocampus to cued and contextual fear conditioning, Behav. Neurosci. 106 (1992) 274–285.
[44] T. Lu, Y. Pan, S.Y. Kao, C. Li, I. Kohane, J. Chan, B.A. Yankner, Gene regulation and DNA damage in the ageing human brain, Nature 429 (2004) 883–891.
[45] U. Rass, I. Ahel, S.C. West, Defective DNA repair and neurodegenerative disease, Cell 130 (2007) 991–1004.
[46] T. Nouspikel, P.C. Hanawalt, When parsimony backfires: neglecting DNA repair may doom neurons in Alzheimer's disease, Bioessays 25 (2003) 168–173.
[47] S. Krantic, N. Mechawar, S. Reix, R. Quirion, Apoptosis-inducing factor: a matter of neuron life and death, Prog. Neurobiol. 81 (2007) 179–196.
[48] M. Sedarous, E. Keramaris, M. O'Hare, E. Melloni, R.S. Slack, J.S. Elce, P.A. Greer, D.S. Park, Calpains mediate p53 activation and neuronal death evoked by DNA damage, J. Biol. Chem. 278 (2003) 26031–26038.
[49] W. Xu, T.P. Wong, N. Chery, T. Gaertner, Y.T. Wang, M. Baudry, Calpain-mediated mGluR1alpha truncation: a key step in excitotoxicity, Neuron 53 (2007) 399–412.
[50] J. Zhu, W. Li, Z. Mao, Cdk5: mediator of neuronal development, death and the response to DNA damage, Mech. Ageing Dev. 132 (2011) 389–394.
[51] D. Qu, J. Rashidian, M.P. Mount, H. Aleyasin, M. Parsanejad, A. Lira, E. Haque, Y. Zhang, S. Callaghan, M. Daigle, M.W. Rousseaux, R.S. Slack, P.R. Albert, I. Vincent, J. M. Woulfe, D.S. Park, Role of Cdk5-mediated phosphorylation of Prx2 in MPTP toxicity and Parkinson's disease, Neuron 55 (2007) 37–52.
[52] E. Huang, D. Qu, Y. Zhang, K. Venderova, M.E. Haque, M.W. Rousseaux, R.S. Slack, J.M. Woulfe, D.S. Park, The role of Cdk5-mediated apurinic/apyrimidinic endonuclease 1 phosphorylation in neuronal death, Nat. Cell Biol. 12 (2010) 563–571.
[53] D.S. Park, B. Levine, G. Ferrari, L.A. Greene, Cyclin dependent kinase inhibitors and dominant negative cyclin dependent kinase 4 and 6 promote survival of NGF-deprived sympathetic neurons, J. Neurosci. 17 (1997) 8975–8983.
[54] A. Copani, D. Uberti, M.A. Sortino, V. Bruno, F. Nicoletti, M. Memo, Activation of cell-cycle-associated proteins in neuronal death: a mandatory or dispensable path? Trends Neurosci. 24 (2001) 25–31.
[55] F. Zindy, J.J. Cunningham, C.J. Sherr, S. Jogal, R.J. Smeyne, M.F. Roussel, Postnatal neuronal proliferation in mice lacking Ink4d and Kip1 inhibitors of cyclin-dependent kinases, Proc. Natl. Acad. Sci. U. S. A. 96 (1999) 13462–13467.
[56] G. Thiel, G. Cibelli, Regulation of life and death by the zinc finger transcription factor Egr-1, J. Cell. Physiol. 193 (2002) 287–292.
[57] B.A. Yankner, T. Lu, P. Loerch, The aging brain, Annu. Rev. Pathol. 3 (2008) 41–66.
[58] M. Ljungman, D.P. Lane, Transcription — guarding the genome by sensing DNA damage, Nat. Rev. Cancer 4 (2004) 727–737.